



## Research paper

## Pt(IV) complexes conjugating with chalcone analogue as inhibitors of microtubule polymerization exhibited selective inhibition in human cancer cells



Xiaochao Huang<sup>a,1</sup>, Rizhen Huang<sup>a,1</sup>, Zhimei Wang<sup>a</sup>, Lingxue Li<sup>a</sup>, Shaohua Gou<sup>a,\*</sup>, Zhixin Liao<sup>a</sup>, Hengshan Wang<sup>b,\*\*</sup>

<sup>a</sup> Jiangsu Province Hi-Tech Key Laboratory for Biomedical Research, Southeast University, Nanjing 211189, China

<sup>b</sup> State Key Laboratory for the Chemistry and Molecular Engineering of Medicinal Resources (Ministry of Education of China), School of Chemistry and Pharmaceutical Sciences of Guangxi Normal University, Guilin 541004, China

## ARTICLE INFO

## Article history:

Received 25 May 2017

Received in revised form

17 September 2017

Accepted 23 January 2018

Available online 4 February 2018

## Keywords:

Anticancer activity

Pt(IV) complex

Tubulin polymerization

Apoptosis

## ABSTRACT

Six novel of Pt(IV) complexes comprising chalcone analogues were synthesized and evaluated for anti-proliferative activity using MTT assay. *In vitro* evaluation revealed that all Pt(IV) complexes showed better and more potent activity against three human cancer cells including CDDP resistant cells than that of their corresponding mother Pt(II) species. Among them, two representative complexes, **14** and **17**, exhibited better cell selectivity between cancer cells and normal cells than CDDP. Molecular docking study indicated that complexes **14** and **17** could bind to the colchicine site of tubulin. Moreover, complexes **14** and **17** also remarkably displayed inhibition of cell migration against HUVEC cells *in vitro*. Molecular mechanism studies suggested that **14** and **17** induced production of reactive oxygen species (ROS), cell cycle arrest at the G2/M phase, and mitochondria-mediated apoptosis by regulating the expression of Bcl-2 family members.

© 2018 Elsevier Masson SAS. All rights reserved.

## 1. Introduction

Cisplatin (CDDP), carboplatin and oxaliplatin (OXP) (Fig. 1) as Pt(II)-based anticancer drugs approved by FDA have been widely used for the treatment of a variety of cancers in the clinical [1–5]. However, the development of drug resistance, side effects and high toxicity have rendered CDDP and its analogues suboptimum for clinical applications [6–9]. Therefore, great efforts have been devoted to the design of novel and effective platinum based drugs for overcoming the above mentioned shortcomings [10,11]. In the past several decades, thousands of Pt(II) complexes have been synthesized and screened for anticancer activity, but only a small number of compounds were used in clinical trials and most of them turned out to be invalid [12]. Hence, use of Pt(IV) complexes as prodrugs is presently one of strategies to overcome the drawbacks including low bioavailability, severe side effects and acquired

resistance of CDDP [10,11]. In contrast to their Pt(II) counterparts, Pt(IV) complexes with a low-spin, d<sup>6</sup> octahedral geometry displaying kinetic inertness are expected to exhibit great promise in the search for the next generation of platinum drugs, because they can be easily reduced to their Pt(II) equivalents by intracellular reducing molecules such as ascorbic acid or glutathione [11,13]. So far, there have been several reports on Pt(IV) complexes including those with active pharmacophores, which were used as prodrugs to improve the antitumor activity and overcome the side effect of CDDP (Fig. 2) [14–19].

Microtubules, formed through polymerization of  $\alpha$ - and  $\beta$ -tubulin heterodimers, are crucial to a large number of fundamental cell functions, such as cell replication, maintenance of cell shape, intracellular transport and migration [20–22]. Since microtubules play a major role in mitosis, they have been recognized as an important target for the development of novel antitumor agents in anticancer chemotherapy (Fig. 3) [23–25]. Generally speaking, the inhibitors of microtubule can be divided into two major types: microtubule destabilizers including combretastatin A-4, colchicine, and vinca alkaloids, and microtubule stabilizers like taxanes [26,27]. Up to now, the inhibitors of tubulin including taxanes,

\* Corresponding author.

\*\* Corresponding author.

E-mail addresses: [sgou@seu.edu.cn](mailto:sgou@seu.edu.cn) (S. Gou), [whengshan@163.com](mailto:whengshan@163.com) (H. Wang).

<sup>1</sup> Co-first author: These authors contributed equally to this work.

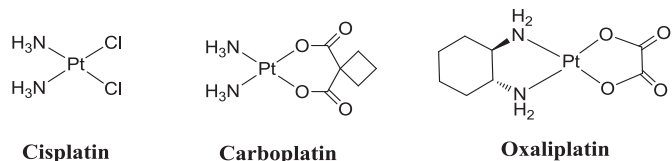


Fig. 1. FDA approved Pt(II) anticancer agents.

vinca alkaloids and paclitaxel are forceful as anti-mitotic agents, and they have been widely used against certain types of malignancies in the past decades [28,29]. Unfortunately, high toxicity,

side effects, poor solubility, the development of drug resistance, low oral bioavailability and complicated synthesis have always limited these compounds' using in the clinical treatment of solid tumors. Recent studies suggested that the combination of platinum anticancer agents with tubulin inhibitors including paclitaxel and docetaxel can result in the improvement of therapeutic efficacy [30]. In recent years, chalcone and its analogues have been found to exhibit potent cytotoxicity against a large number of human cancer cells including multidrug resistant cancer cell lines and strongly inhibit tubulin polymerization by binding to the colchicine binding site [31–36]. In addition, the chalcone derivatives **1a** and **2a** (Fig. 3), served as inhibitor of microtubule polymerization, displayed good

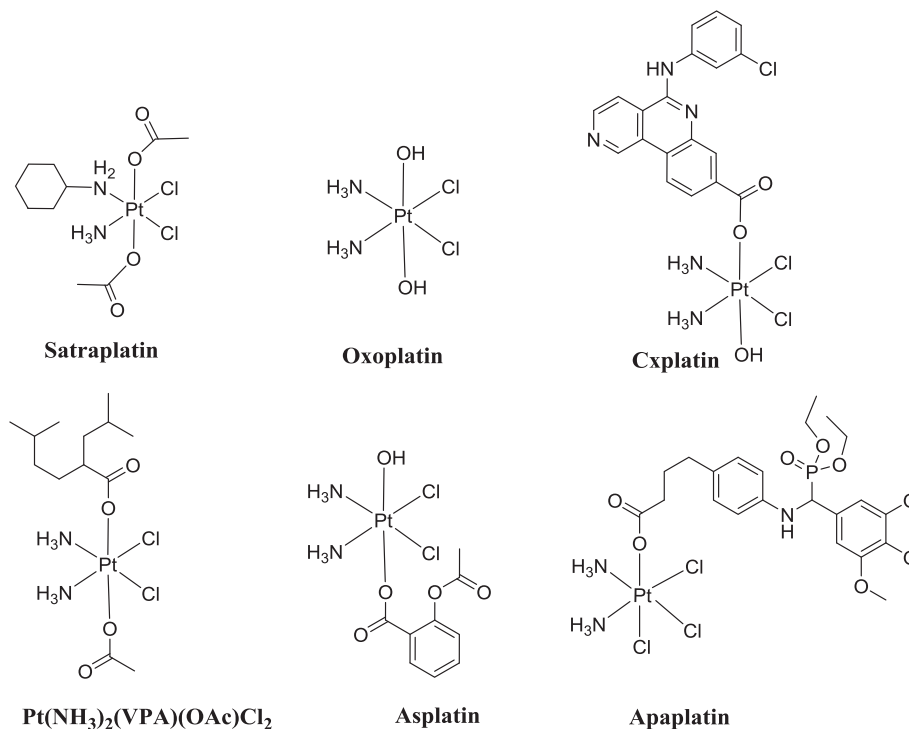
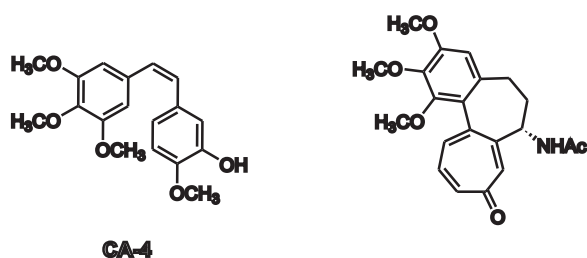


Fig. 2. Chemical structures of some Pt(IV) complexes prodrugs.



antitumor activity against human cancer cell lines [37–39]. Moreover, Schobert and co-workers recently showed that the Pt(II) complex conjugating with **2a** and its derivatives exhibited moderate antitumor activities against diverse human cancer cells owing to the different mode of actions such as DNA-targeting Pt(II) complexes and tubulin-targeting chalcone moieties [39]. Hence, a combination of tubulin inhibitors with cytotoxic DNA damaging platinum-based agents can be considered as a fascinating strategy for targeting tubulin and DNA, and at least in theory, can effectively improve the antitumor activities of platinum drugs and overcome their adverse side effects. However, up to now, no example of a prodrug containing both CDDP and the chalcone derivative has been reported as an inhibitor of tubulin polymerization. In this paper, a series of Pt(IV) prodrugs containing chalcone derivatives as an axial ligand in the octahedrally geometric Pt(IV) atom were designed, synthesized and evaluated for antitumor activity. Among these Pt(IV) complexes, complexes **14** and **17** displayed excellent anticancer activity against the tested cancer cell lines including CDDP-resistant cell line A549. The mechanism action of the potent Pt(IV) complexes **14** and **17** was investigated. In short, these studies obviously suggested that the anti-proliferative activity of the typical complex was significantly more potent than that of CDDP due to the synergism of conjugating DNA damaging platinum-based agents and tubulin-targeting chalcone moieties.

## 2. Results and discussion

### 2.1. Chemistry

#### 2.1.1. Synthesis of target compounds

The general steps to synthesize the target compounds have been outlined in Scheme 1. Pt(IV) complexes **11–13** were prepared according to the reported procedures [18,40]. First, by Claisen-Schmidt condensation of **1** with **2** in the presence of 50% KOH in CH<sub>3</sub>OH to produce the key intermediate **3**, and then treating with Fe powder and NH<sub>4</sub>Cl in ethanol/water easily yielded compound **4**. Subsequently, intermediate **7** or **8** was achieved by the formation of amide bond between **5** or **6** and **4**, respectively, in the presence of HOBt/EDCI, then **7** or **8** followed by its hydrolysis with aluminum hydroxide in the presence of THF/H<sub>2</sub>O to obtain the acid **9** or **10**. Finally, the synthesis of target compounds (**14–19**) obtained by esterification reactions between **9**, or **10** and Pt(IV) precursor complexes **11–13**, respectively, in the presence of TBTU/Et<sub>3</sub>N.

#### 2.1.2. Characterization

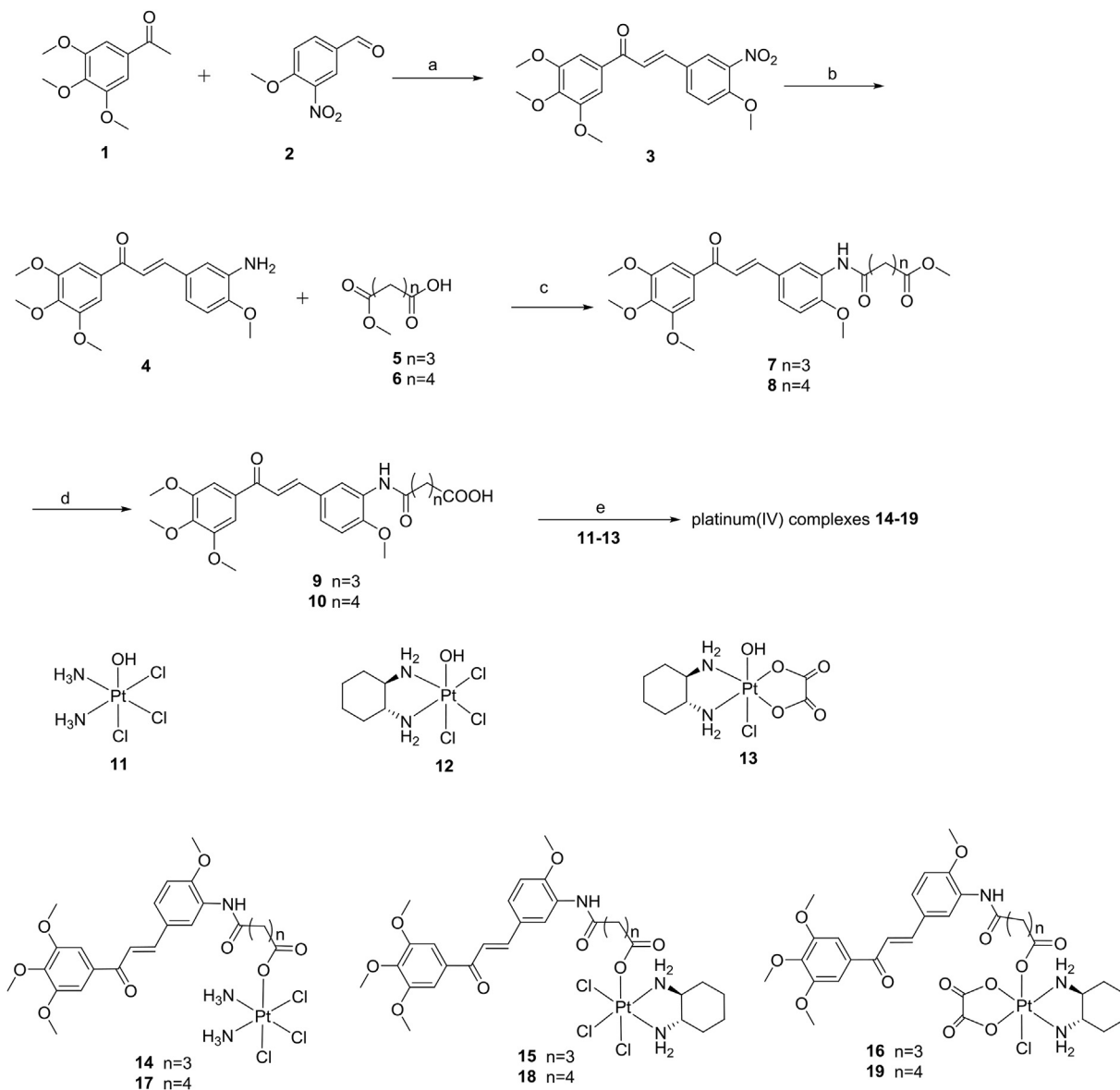
The chemical structures of these target Pt(IV) complexes were confirmed by IR, <sup>1</sup>H NMR, <sup>13</sup>C NMR, <sup>195</sup>Pt NMR, elemental analysis and high resolution mass spectra (HR-MS). The [M+H]<sup>+</sup> parent ions of compounds **3**, **4**, **7**, **8** and the [M+Cl]<sup>-</sup> parent ions of compound **17** and the [M-H]<sup>-</sup> parent ions of compounds **9**, **10**, **14**, **15**, **16**, **18** and **19** were observed using HR-ESI-MS. The IR spectrum showed characteristic absorption bands for 1653 cm<sup>-1</sup> (C=O) and 1577 and 1457 cm<sup>-1</sup> (aromatic ring) and 1354 cm<sup>-1</sup> (NO<sub>2</sub>) (**3**) and 1650 cm<sup>-1</sup> (C=O) and 3444 and 3358 cm<sup>-1</sup> (NH<sub>2</sub>) (**4**) functionalities. In the <sup>1</sup>H NMR spectrum (**3**), the proton signals at δ 7.75 (d, *J* = 15.3 Hz, 1H) and 7.43 (d, *J* = 15.6 Hz, 1H) suggested the presence of one trans-substituted double bond segment, and the characteristic resonances of four methoxy [δ<sub>H</sub> 4.02 (3H, s), 3.96 (6H, s), 3.95 (3H, s)] groups were also observed. The <sup>1</sup>H NMR spectroscopic data of compound **4** was very similar to compound **3**. We could observe characteristic resonances by <sup>13</sup>C NMR at δ<sub>C</sub> 188.42 (**3**) and 189.42 (**4**) were assigned to the carbonyl group, respectively. In addition, the IR and <sup>1</sup>H NMR spectroscopic data of compounds **7** and **8** were similar to compound **4**, except for the presence of an amide bond [the proton signals at δ<sub>H</sub> 8.81 (s, 1H) for compounds **7** and **8**], and

the connectivity of the aliphatic chain [(CH<sub>2</sub>)<sub>3</sub> or (CH<sub>2</sub>)<sub>4</sub>] to the chalcone moiety [the proton signals at δ<sub>H</sub> 2.53–2.45 (m, 4H), 2.13–2.03 (m, 2H) for compound **7** and 2.48–2.36 (m, 4H), 1.83–1.73 (m, 4H) for compound **8**], and its molecular formula was established as C<sub>25</sub>H<sub>29</sub>NO<sub>8</sub> (**7**) and C<sub>26</sub>H<sub>31</sub>NO<sub>8</sub> (**8**) on the basis of the HR-ESI-MS data (*m/z* 472.18732 and 486.20171, [M+H]<sup>+</sup>), respectively. Furthermore, <sup>13</sup>C NMR resonances for carbonyl group were observed at δ<sub>C</sub> 189.43, 173.54 and 170.59 (**7**) and 189.45, 173.80 and 170.99 (**8**). For compounds **9** and **10**, the molecular formula was assigned as C<sub>24</sub>H<sub>27</sub>NO<sub>8</sub> and C<sub>25</sub>H<sub>29</sub>NO<sub>8</sub> on the basis of the HR-ESI-MS data (*m/z* 456.16883 (**9**) and 470.22474 (**10**), [M-H]<sup>-</sup>), and the <sup>1</sup>H NMR spectroscopic data of compounds **9** and **10** displayed a single peak at δ<sub>H</sub> 11.90 (**9**) and 11.99 (**10**) suggested the presence of carboxylic acid group (-COOH), respectively. All the HR-ESI-MS spectra of the Pt(IV) complexes (**14–19**) gave main peaks corresponding to [M-H]<sup>-</sup> or [M+Cl]<sup>-</sup> ions, which were composed of a few isotopic peaks due to the presence of platinum isotopes, and characteristic resonances could be observed at δ 544.37 (**14**), 412.26 (**15**), 1000.02 (**16**), 544.67 (**17**), 414.26 (**18**) and 996.61 (**19**) in <sup>195</sup>Pt NMR, suggested the bonding between the Pt(IV) ions and the ligands. In addition, <sup>1</sup>H NMR spectroscopic data of **14** and **17** were similar to **9** and **10**, except for characteristic resonances at δ 6.52–5.70 (m, 6H) for **14** and 6.45–5.76 (m, 6H) for **17** of (NH<sub>3</sub>)<sub>2</sub> in <sup>1</sup>H NMR and were assigned to the CDDP core, and a single peak (-COOH) disappears compared to **9** and **10**, respectively. For complexes **15** and **18**, characteristic resonances at δ<sub>H</sub> 9.60–9.56 (m, 1H), 8.14 (s, 1H), 7.79 (s, 1H) and 7.73–7.70 (m, 1H) for **15** and 9.64–9.59 (m, 1H), 8.13 (s, 1H), 7.78 (s, 1H) and 7.73–7.71 (m, 1H) for **18** of (NH<sub>2</sub>)<sub>2</sub> in <sup>1</sup>H NMR and were assigned to the DACHPt core, and resonances at δ<sub>H</sub> 2.76–2.70 (m, 2H), 2.19–2.04 (m, 1H), 1.55–1.48 (m, 3H), 1.31–1.06 (m, 3H) for **15** and 2.75–2.69 (m, 2H), 2.19–2.03 (m, 2H), 1.55–1.46 (m, 3H), 1.32–1.04 (m, 3H) for **18** of (CH<sub>2</sub>)<sub>4</sub> or (NH<sub>2</sub>CH)<sub>2</sub> in <sup>1</sup>H NMR and were assigned to the DACHPt core, respectively. The <sup>1</sup>H and <sup>13</sup>C NMR spectroscopic data of **16** and **19** were similar to **15** and **18**, except for characteristic resonances at δ<sub>C</sub> 163.82 (**16**) and 163.69 (**19**) of the carbonyl group in <sup>13</sup>C NMR and were assigned to the OXP core compared to **15** and **18**. Moreover, the far-IR spectrum of the target Pt(IV) complexes **14–19** displayed characteristic absorption bands of Pt-Cl in the range from 321 to 361 cm<sup>-1</sup>, and the Pt-N stretches in the region between 434 and 456 cm<sup>-1</sup>. In addition, in all complexes the Pt-O stretches in the range 525–575 cm<sup>-1</sup> were also observed.

### 2.2. Biological evaluation

#### 2.2.1. Cytotoxicity test

The cytotoxic activity of compounds **9–10** and **14–19** was evaluated *in vitro* against three human cancer cell lines (HepG-2, hepatoma; SK-OV-3, ovarian; NCI-H460, lung), and two human normal cell lines (HL-7702, liver; BEAS-2B, lung) with CDDP, OXP, DACHPt, and compound **4** as reference controls using the MTT assay. The biological results of the compounds are summarized in Table 1. As shown in Table 1, compounds **9** and **10** showed lower cytotoxicity against the tested cancer cells than that of positive drug compound **4**. However, complexes **14–16** and **17–19**, the Pt(IV) derivatives of CDDP, DACHPt or OXP with one chalcone derivative **9** or **10** ligand in the axial position, displayed significant antitumor activity against all tested cell lines. Complexes **14** and **17**, Pt(IV) derivatives of CDDP, owned up to 2.71-fold and 5.54-fold increased cytotoxicity compared with CDDP in SK-OV-3 cells, significantly exhibiting more effective antitumor activity than compound **4**. It was also noticed that complexes **14** and **17** showed high sensitivity toward HepG-2 and NCI-H460 cancer cells with IC<sub>50</sub> values of 2.23, 4.65 and 0.97, 3.66 μM, but low cytotoxicity toward two normal cells HL-7702 and BEAS-2B with IC<sub>50</sub> values of 24.56,



**Scheme 1.** Synthetic route of the Pt(IV) complexes. Reagents and conditions: (a) 50% KOH/H<sub>2</sub>O, MeOH, 0 °C; (b) Fe, NH<sub>4</sub>Cl, EtOH, 85 °C; (c) EDCI, DMAP, CH<sub>2</sub>Cl<sub>2</sub>, room temperature; (d) LiOH·H<sub>2</sub>O, THF/H<sub>2</sub>O, room temperature; (e) TBTU, Et<sub>3</sub>N, DMF, room temperature.

34.47 and 33.16, 35.14 μM compared with the positive drug CDDP (8.51, 10.42 μM), respectively. Therefore, the selectivity index of complexes **14** and **17** were calculated out as 11.05, 7.41 and 34.19, 9.34, respectively, much higher than that of CDDP (0.94 and 0.93). The similar trend was also observed in complexes **15–16** and **18–19**. Interestingly, complexes **14–16** have a different carbon chain from complexes **17–19**, the corresponding compounds displayed different antitumor activities that are enhanced with an increase of the carbon chain length. Moreover, all Pt(IV) complexes showed obvious lower cytotoxicity than those of their corresponding Pt(II) positive controls (CDDP, DACHPt and OXP) against two human normal cells, suggesting that these Pt(IV) complexes displayed better cell selectivity between cancer cells and normal liver cells than their mother Pt(II) agents.

#### 2.2.2. Antitumor activity of target complexes against CDDP resistant cancer cell line

Drug resistance is a major therapeutic problem that confined

the efficacies of CDDP for different human cancer cells. According to the above biological results, we further evaluated the cytotoxicity of complexes **14–17** against CDDP sensitive and resistant cancer cells (human lung epithelial cells A549 and A549/CDDP). The biological results of the compounds are shown in Table 2 and Fig. 4 A. As shown in Table 2, the IC<sub>50</sub> value of CDDP against A549/CDDP resistant cells was increased to 42.51 μM. However, the activity of complexes **14** and **17** was not obviously changed for the CDDP resistant cancer cells when compared with the CDDP sensitive cells. IC<sub>50</sub> values of **14** and **17** against CDDP resistant A549 cells were 4.25 and 3.05 μM, respectively. It was much significant to discover that complexes **14** and **17** had much lower resistance factors (1.15 and 1.26) than that of CDDP (4.95). Moreover, other Pt(IV) complexes **15–16** and **18–19** also exhibited obvious anticancer activities against the CDDP resistant A549/CDDP cells comparable to those of DACHPt and oxaliplatin with small resistance factors. The results indicated that these Pt(IV) complexes might be useful in the treatment of drug refractory cancer resistance to other platinum

**Table 1**  
Cytotoxic effects of Pt(IV) complexes on human cancer and normal cell lines.

Comp.	IC <sub>50</sub> (μM) <sup>d</sup>						
	HepG-2	SK-OV-3	NCI-H460	HL-7702	BEAS-2B	SI <sup>e</sup>	SI <sup>f</sup>
<b>4</b>	10.88 ± 2.11	5.46 ± 1.03	8.43 ± 2.17	15.07 ± 2.73	18.43 ± 2.38	1.39	2.18
<b>9</b>	35.04 ± 3.08	20.21 ± 2.15	45.09 ± 3.43	55.38 ± 3.29	48.39 ± 3.16	1.58	1.08
<b>10</b>	25.85 ± 3.07	15.43 ± 2.35	35.43 ± 2.91	65.43 ± 3.26	48.42 ± 3.18	2.53	1.37
<b>14</b>	2.23 ± 0.39	2.75 ± 1.06	4.65 ± 1.12	24.65 ± 2.13	34.47 ± 3.11	11.05	7.41
<b>15</b>	6.25 ± 1.28	6.78 ± 1.89	5.29 ± 2.07	37.29 ± 3.15	45.43 ± 3.73	5.97	8.59
<b>16</b>	13.12 ± 2.13	9.85 ± 2.54	14.22 ± 2.03	41.22 ± 2.94	44.91 ± 4.01	3.14	3.16
<b>17</b>	0.97 ± 0.25	2.11 ± 0.38	3.66 ± 0.77	33.16 ± 2.51	35.14 ± 2.38	34.19	9.34
<b>18</b>	3.81 ± 0.91	5.56 ± 0.67	4.61 ± 1.06	44.61 ± 4.02	41.69 ± 3.05	11.70	9.04
<b>19</b>	10.21 ± 1.01	8.52 ± 1.19	10.38 ± 2.35	48.54 ± 3.61	49.08 ± 2.33	4.75	4.72
CDDP <sup>a</sup>	9.05 ± 1.23	7.46 ± 1.48	11.21 ± 1.71	8.51 ± 3.61	10.42 ± 1.92	0.94	0.93
DACHPt <sup>b</sup>	10.50 ± 2.01	9.03 ± 0.81	9.58 ± 1.16	7.61 ± 1.83	8.55 ± 1.36	0.72	0.89
OXPC <sup>c</sup>	15.58 ± 3.13	12.06 ± 1.66	16.09 ± 2.44	10.25 ± 1.95	12.13 ± 2.41	0.66	0.75

<sup>a</sup> Cisplatin.<sup>b</sup> Dichloro(1*R*,2*R*-diaminocyclohexane)platinum(II).<sup>c</sup> Oxaliplatin.<sup>d</sup> *In vitro* cytotoxicity was determined by MTT assay upon incubation of the live cells with the compounds for 72 h.<sup>e</sup> Selectivity Index = IC<sub>50</sub>(HL-7702)/IC<sub>50</sub>(HepG-2).<sup>f</sup> Selectivity Index = IC<sub>50</sub>(BEAS-2B)/IC<sub>50</sub>(NCI-H460). Mean values based on three independent experiments.**Table 2**  
Biological activity of Pt(IV) complexes against cisplatin sensitive and resistant cancer cells (A549 and A549/CDDP).

Comp.	IC <sub>50</sub> (μM) <sup>d</sup>		
	A549	A549/CDDP	R F <sup>e</sup>
<b>4</b>	5.61 ± 1.36	6.55 ± 2.08	1.17
<b>9</b>	27.11 ± 2.81	32.11 ± 3.09	1.18
<b>10</b>	15.51 ± 2.33	19.82 ± 1.89	1.28
<b>14</b>	3.69 ± 0.57	4.25 ± 0.34	1.15
<b>15</b>	6.83 ± 1.01	8.23 ± 1.27	1.20
<b>16</b>	10.15 ± 0.38	12.05 ± 2.04	1.19
<b>17</b>	2.42 ± 0.25	3.05 ± 0.53	1.26
<b>18</b>	4.50 ± 1.09	6.01 ± 1.15	1.34
<b>19</b>	8.51 ± 1.61	10.29 ± 1.07	1.21
CDDP <sup>a</sup>	8.59 ± 1.52	42.51 ± 3.15	4.95
DACHPt <sup>b</sup>	8.65 ± 1.31	21.29 ± 2.68	2.46
OXPC <sup>c</sup>	11.95 ± 1.43	23.76 ± 3.34	1.99

<sup>a</sup> Cisplatin.<sup>b</sup> Dichloro(1*R*,2*R*-diaminocyclohexane)platinum(II).<sup>c</sup> Oxaliplatin.<sup>d</sup> *In vitro* cytotoxicity was determined by MTT assay upon incubation of the live cells with the compounds for 72 h.<sup>e</sup> RF (resistant factor) is defined as IC<sub>50</sub> in A549CDDP/IC<sub>50</sub> in A549. Mean values based on three independent experiments, and the results of the representative experiments are shown.

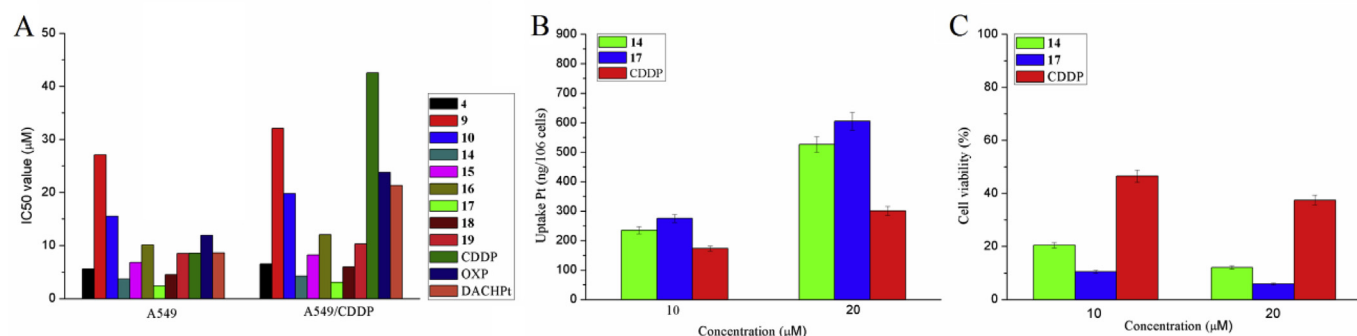
drugs.

### 2.2.3. Cellular uptake

Because Pt(IV) complexes **14** and **17** exhibited better cytotoxicity, they were further typically selected to carry out the cellular uptake test in HepG-2 cells by using the inductively coupled plasma mass spectrometry (ICP-MS). As shown in Fig. 4 B and Table 3, treating HepG-2 cells with complexes **14** and **17** (10.0 and 20.0 μM) for 24 h resulted in an abundant increase in the content of cellular platinum at a dose-dependent manner, showing facile internalization of the complexes within 24 h. Especially, the uptake of two complexes was remarkably higher than that of CDDP. After exposed to 20.0 μM of complex **17** for 24 h, the concentration of cellular platinum rose to 605 ng/10<sup>6</sup> cells, which was two times as much as that of CDDP. Based on the data from both cytotoxicity assay and cellular uptake tests, it is concluded that the improved cellular uptake can lead to the enhance of the antitumor activity.

### 2.2.4. Cell viability

The effect of complexes **14** and **17** on cell proliferation after 72 h treatment were checked in HepG-2 cancer cells using the MTT assay. The biological results of the complexes **14** and **17** are shown in Fig. 4 C. Our results indicated that the Pt(IV) complexes **14** and **17**

**Fig. 4.** (A) IC<sub>50</sub> values of target compounds in A549 and A549/CDDP cancer cells. (B) Intracellular accumulation of CDDP, **14** and **17** (10, 20 μM) in Bel-7404 cells after 24 h. Each value is in nanograms of platinum per 10<sup>6</sup> cells. (C) *In vitro* cytotoxicity of **14**, **17** and CDDP to HepG-2 cancer cells at the same concentration for 72 h. Results are expressed as the mean ± SD for three independent experiments. P < 0.05.

**Table 3**  
Cellular uptake of Pt(IV) complexes **14** and **17** in HepG-2 cells after 24 h of incubation.

	Pt content (ng/10 <sup>6</sup> cells)
Complexes	HepG-2
<b>14</b> (10 μM)	235 ± 23
<b>14</b> (20 μM)	526 ± 54
<b>17</b> (10 μM)	275 ± 31
<b>17</b> (20 μM)	605 ± 62
Cisplatin (10 μM)	173 ± 19
Cisplatin (20 μM)	301 ± 36

The experiments were performed three times, and the results of the representative experiments are shown.

more effectively inhibited cell proliferation in HepG-2 cells than that of CDDP under the same condition (10 and 20 μM), respectively. (Fig. 4 C).

### 2.2.5. Complexes **14** and **17** induced apoptosis in HepG-2 cells

It is well-known that most metal complex anticancer drugs generally kill tumor cells by activating apoptosis [41,42]. Since complexes **14** and **17** were also found to exhibit broad spectrum antitumor activity against all tested human cancer cells and the best activity against HepG-2 cancer cells *in vitro*, they were chosen to be further investigated on the mechanism of action. The induction of apoptosis of HepG-2 cells by complexes **14** and **17** was studied using FITC-Annexin V staining, in which Q1, Q2, Q3, and Q4 represent four different cell states: necrotic cells, late apoptotic or necrotic cells, apoptotic cells and living cells, respectively. HepG-2 cells were treated with **14**, **17**, **4**, CDDP and CDDP/**4** mixture under the same concentration (10 μM) for 24 h, respectively. As shown in Fig. 5, the percentage of cell apoptosis was 0.18% for the control, and cell apoptosis was added up to 16.62% and 19.99%, respectively, at 10 μM of CDDP and **4**, while cells treated with CDDP/**4** mixture (10 μM), the percentage of cell apoptosis was increased to 30.99%. However, the percentage of cell apoptosis was added up to 41.21% and 47.01%, respectively, when cells were treated with Pt(IV) complexes **14** and **17** at 10 μM. Taken together, these results clearly suggested that complexes **14** and **17** could effectively induce apoptosis in HepG-2 cancer cells at the concentration of 10 μM. Interestingly, complex **17** was found to be more effectively inducing apoptosis in human HepG-2 cancer cells than complex **14** under the same condition, hinting that butyl carbon chain in **17** can improve the antitumor activity better than propargyl carbon chain in **14**. The result is compatible to the data obtained from cytotoxicity assay and cellular uptake tests.

### 2.2.6. AO/EB double staining

Apoptosis was further investigated by acridine orange (AO) and ethidium bromide (EB) double staining. Viable cells stained by AO and EB exhibited bright green fluorescence, while the apoptotic cells stained by AO and EB displayed bright orange fluorescence. HepG-2 cells were treated with CDDP/**4**, **14** and **17**, respectively, at the same concentration (10 μM) for 24 h, and untreated HepG-2 cells were used as a negative control and cells treated with CDDP and **4** were used as positive controls. As shown in Fig. 6, complexes **14** and **17** were also confirmed to be able to induce apoptosis in HepG-2 cells.

### 2.2.7. Cell cycle analysis

To study the effect of the synthetic Pt(IV) complexes on the cell growth and division, we used flow cytometry to evaluate the cell cycle distribution of HepG-2 cells following a 48 h treatment with CDDP/**4**, **14** and **17** at 10 μM. Untreated cells were used as a negative control, and cells treated with CDDP and **4** were used as positive

controls. As shown in Fig. 7, in the control group, 5.86% of the HepG-2 cells were in the G2/M phase. It was observed that 21.66% and 19.86% proportion of cells were in the G2/M phase, when treated with 10 μM CDDP and compound **4** for 48 h, respectively. Notably, after treatment with CDDP/**4** mixture at 10 μM, the percentage of cells in the G2/M phase increased to 76.14%. Interestingly, it was significant to observe that complexes **14** and **17** were also effective in arresting the cell cycle at G2/M phase. After treatment with 10 μM complexes **14** and **17** for 48 h, the percentage of cells in the G2/M phase increased to 79.77% and 85.13%, respectively. In short, these results demonstrated that complexes **14** and **17** could induce cell cycle arrest at the G2/M phase.

### 2.2.8. Molecular docking

To gain better understanding on the potency of the synthesized Pt(IV) complexes **14** and **17**, we proceeded to examine the interaction of **14** and **17** with tubulin crystal structure (PDB code: 1SAO) using Sybyl-X 2.0 on a Windows workstation. The binding modes of compounds **14**, **17** and **4** in the colchicine binding site of tubulin are depicted in Fig. 8 and the docking scores obtained are shown in Table 4. The Surflex docking scores are 8.70 for **14**, 11.11 for **17** and 6.59 for **4**, where higher scores indicate greater binding affinity. As the biological activity studies suggested that complexes **14** and **17** were potent, hence, the docking detail of these two compounds were examined for their interactions in ATP binding pocket of tubulin.

Fig. 8 A shows that the interacting mode of compound **14** with the chalcone moiety in the binding site is surrounded by THR327, ALA326, THR181, GLY45 and ASN76. In particular, compound **14** forms five hydrogen bonds with the polar amino acids ASP150, SER151, LEU175, GLU43 and VAL179, suggesting a probable strong electrostatic interaction with the protein. In addition, the hydrophobic moiety of **14** is well embedded in a pocket interacting with several hydrophobic residues making **14** bind tightly to tubulin. Not surprisingly, the accommodation of complex **17** in the binding site is similar to **14** (Fig. 8B). Also in this case, docking simulations showed that the chalcone moiety of compound **17** like **14** can also be accommodated in the same hydrophobic groove, adopting an energetically stable conformation. Moreover, the chalcone moiety of compound **17** forms eight hydrogen bonds with the polar amino acids GLU43, VAL179, ASN269, ASP272 and THR327. In addition, the crucial electrostatic interactions between the ammine from the Pt(IV) unit and GLN172, THR327 and ASP272 residues from the neighboring  $\alpha$ -subunit were observed in the binding pocket. Similar interactions with ASP272 or THR327 were observed in the binding mode of compound **4** (Fig. 8C). It is interesting to note that the crucial electrostatic interactions between the methoxy group of the 3,4,5-trimethoxy-phenyl unit and residue VAL179 of the neighboring  $\alpha$ -subunit are observed in the binding pocket, demonstrating a plausible competitive mechanism of action at the colchicine site.

### 2.2.9. Complexes **14** and **17** inhibited the polymerization of tubulin *in vitro*

To further investigate whether the antitumor activities of these Pt(IV) complexes were related to the interaction with the microtubule system, the effect of complexes **14** and **17** on the polymerization of purified tubulin were evaluated at a concentration of 10 μM. Compound **4**, paclitaxel and CA-4 were served as a reference. As illustrated in Fig. 9, paclitaxel (10 μM) was found to stimulate tubulin polymerization, while CA-4 (10 μM) or compound **4** (10 μM) effectively inhibited tubulin polymerization as expected. For complexes **14** and **17**, an obvious inhibition of polymerization was observed at the indicated concentration. More importantly, complex **17** exhibited more significant inhibition tubulin

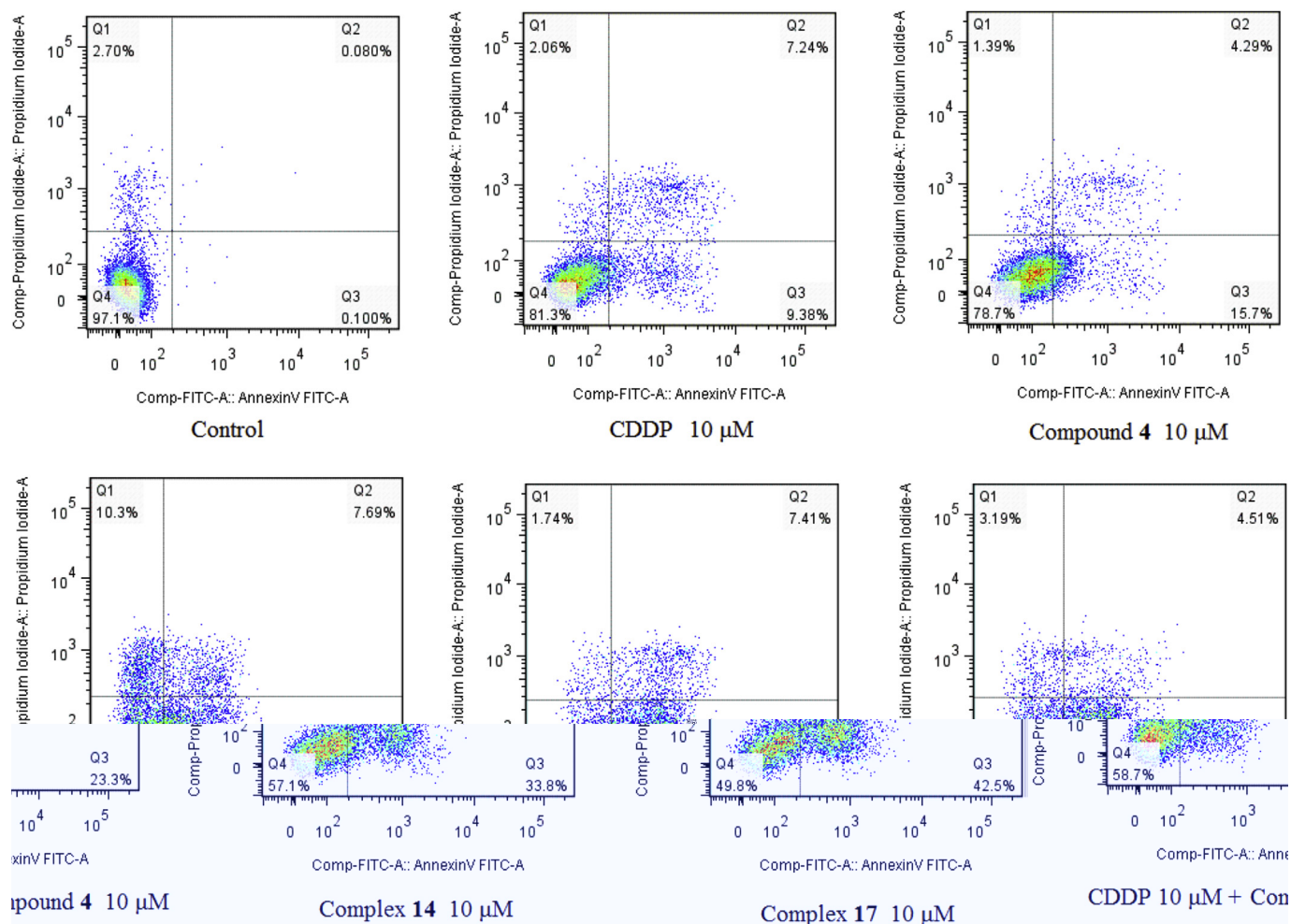


**Fig. 5.** Representative flow cytometry histograms of apoptotic HepG-2 cells after 24 h treatment with CDDP, **4**, CDDP/**4**, **14** and **17** at the indicated concentrations. The cells were harvested and labeled with annexin-V-FITC and PI, and analyzed by flow cytometry. The experiments were performed at least three times, and the results of the representative experiments were shown.

polymerization compared to complex **14**, which indicated the rational relationship between the inhibition of tubulin and the corresponding antitumor activity.

#### 2.2.10. Complexes **14** and **17** triggered ROS generation

Reactive oxygen species (ROS) production are highly harmful elements to cells as they initiate oxidative stress and ultimately cause apoptosis in cancer cells [43,44]. In order to determine whether Pt(IV) complexes **14** and **17** inducing apoptosis was ROS-dependent, HepG-2 cells were treated with **4**, CDDP/**4** mixture, **14** and **17** at the same concentration (10 μM) for 24 h, the fluorescent probe 2,7-dichlorofluorescein diacetate (DCF-DA) was used to detect by flow cytometry. As shown in Fig. 10, the results suggested that complexes **14** and **17** induced the production of significant amounts of ROS in HepG-2 cells. After exposure to 10 μM of complexes **14** and **17** for 24 h, the ROS level was 68.1% and 71.6%, respectively, which were four times as great as those of the control and CDDP. Taken together, these results proved that complexes **14** and **17** caused oxidative imbalance in HepG-2 cells.

#### 2.2.11. Complexes **14** and **17** caused mitochondrial dysfunction through decreasing the mitochondrial membrane potential (MMP)

Mitochondrial dysfunction plays an important role in the progression of apoptosis, which is demonstrated by several vital events

including the reduction of mitochondrial membrane potential (MMP) and the release of cytochrome *c* (Cyt *c*) [45,46]. To further investigate whether apoptosis induced by **14** and **17** was related to mitochondrial dysfunction, flow cytometry analysis was used to detect the MMP using JC-1 staining. As shown in Fig. 11, treatment of HepG-2 cells with **4**, CDDP/**4** mixture, **14** and **17**, respectively, caused a decrease the MMP level at the same concentration (10 μM) for 24 h. These data clearly suggested that both **14** and **17** could effectively induced MMP collapse and eventually triggered apoptotic cell death. Notably, complex **17** was found to be more effectively inducing MMP collapse in human HepG-2 cancer cells than complex **14** under the same condition. The results were consistent well with the previous experimental data, indicating that butyl carbon chain in **17** can enhance the antitumor activity of the target compound better than propargyl carbon chain in **14**.

#### 2.2.12. Complexes **14** and **17** inhibited the migration of HUVEC cell *in vitro*

Metastasis was an important event in later period of cancer progression. Hence, the inhibition of metastasis was critical for efficient cancer treatment. Moreover, migration was a major step during metastasis. Therefore, in this study, we evaluated the inhibition effect of complexes **14** and **17** on cell migration *in vitro* by wound healing assay. As expected, complexes **14** and **17** strongly

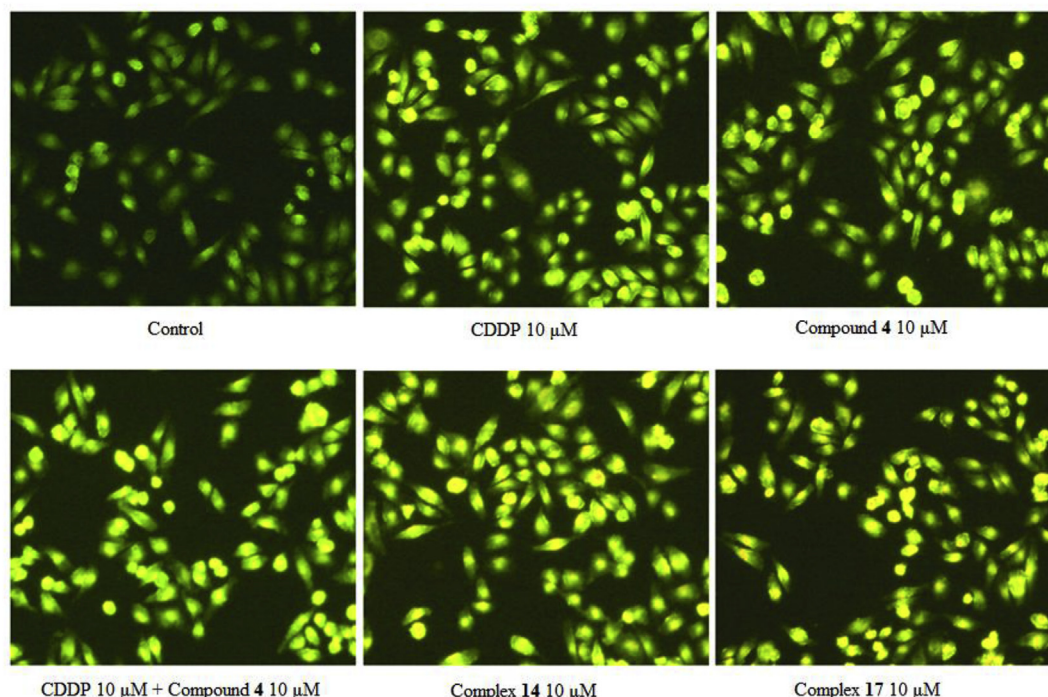


**Fig. 6.** AO/EB double staining was used to detect the apoptosis after HepG-2 cells were exposed at the same concentration of CDDP, **4**, CDDP/**4**, **14** and **17** for 24 h. Untreated cells were used as a negative control and cells treated with CDDP and **4** were used as positive controls for 24 h, respectively. The experiments were performed at least three times, and the results of the representative experiments were shown.

suppressed the migration of HUVEC cells compared with CDDP after 24 h under the same concentration (10  $\mu\text{M}$ ), respectively. The detail is shown in Fig. 12.

#### 2.2.13. Complexes **14** and **17** induced apoptosis via the regulation of apoptosis-related protein expression

Bcl-2 family members are essential components of mitochondrial stress-induced cellular apoptosis [47]. Previously, many reports proposed that metal complexes induced mitochondria mediated apoptosis in cancer cells through the regulation of Bcl-2 family proteins [41,48,49]. Therefore, the expression of apoptosis-related proteins was also investigated for complexes **14** and **17**. Western blot assay demonstrated that these two complexes up-regulated the expression of Bax (pro-apoptotic protein) and correspondingly down-regulated the expression of Bcl-2 (anti-apoptotic protein) at the indicated concentration (Fig. 13). The ratio of Bcl-2/Bax was decreased, resulting in the release of Cyt *c*. Subsequently, Cyt *c* caused activation of downstream caspase-9 and -3. In short, these results proved that complexes **14** and **17** could induce mitochondria mediated apoptosis in HepG-2 cells through regulating the expression of Bcl-2 family members. It was noted again that the change of the expression levels of these proteins for complex **17** was more remarkable than complex **14**, suggesting that the length of carbon chain played an important role in anticancer activity.

### 3. Conclusions

In summary, six Pt(IV) prodrugs derived from CDDP, DACHPt and OXP with two chalcone analogues as an inhibitor of tubulin were designed and synthesized. *In vitro* evaluation revealed that all the resulting Pt(IV) complexes not only displayed better anticancer activities than their mother Pt(II) counterparts against three tested human cancer cells, but also indicated less toxic than their

corresponding Pt(II) complexes against two normal human cells. In addition, all Pt(IV) complexes exhibited certain capability to overcome CDDP drug resistance with low resistance indices when treated with CDDP sensitive cells A549 and CDDP resistant cells A549/CDDP. Two typical compounds, **14** and **17** with different alkyl chain linkers, were chosen for further biological study. Complexes **14** and **17** displayed different antitumor activities and cellular uptake, which can be attributed to the difference of their carbon chain length. It was noted that these two complexes significantly caused cell cycle arrest at G2/M phases and effectively induced cell apoptosis when treated with HepG-2 cells, and they could effectively inhibit cell migration against HUVEC cells *in vitro*. Moreover, the results of tubulin polymerization assay and molecular docking analysis indicated that complexes **14** and **17** could inhibit tubulin polymerization and bind to the colchicine site of tubulin. Molecular mechanism studies suggested that complexes **14** and **17** caused apoptotic cell death of human cancer cells HepG-2 through the mitochondrial mediated pathway by releasing mitochondrial Cyt *c*, down-regulating Bcl-2, up-regulating Bax, which in turn proteolytically activated downstream caspase-9 and caspase-3. Taken together, our study indicated that Pt(IV) anticancer prodrugs containing a tubulin inhibitor moiety can effectively enhance or inhibit tubulin polymerization that may be a promising approach for multiple targeted cancer therapy.

### 4. Experimental section

All chemicals and solvents were analytical reagent grade and commercially available, and used without further purification unless noted specifically. Column chromatography was performed using silica gel (200–300 mesh). Mass spectra were measured on an Agilent 6224 TOF LC/MS instrument. Elemental analyses of C, H, and N used a Vario MICRO CHNOS elemental analyzer (Elementary). Infrared spectra were obtained on a TENSOR27 PMA 50 FT-IR

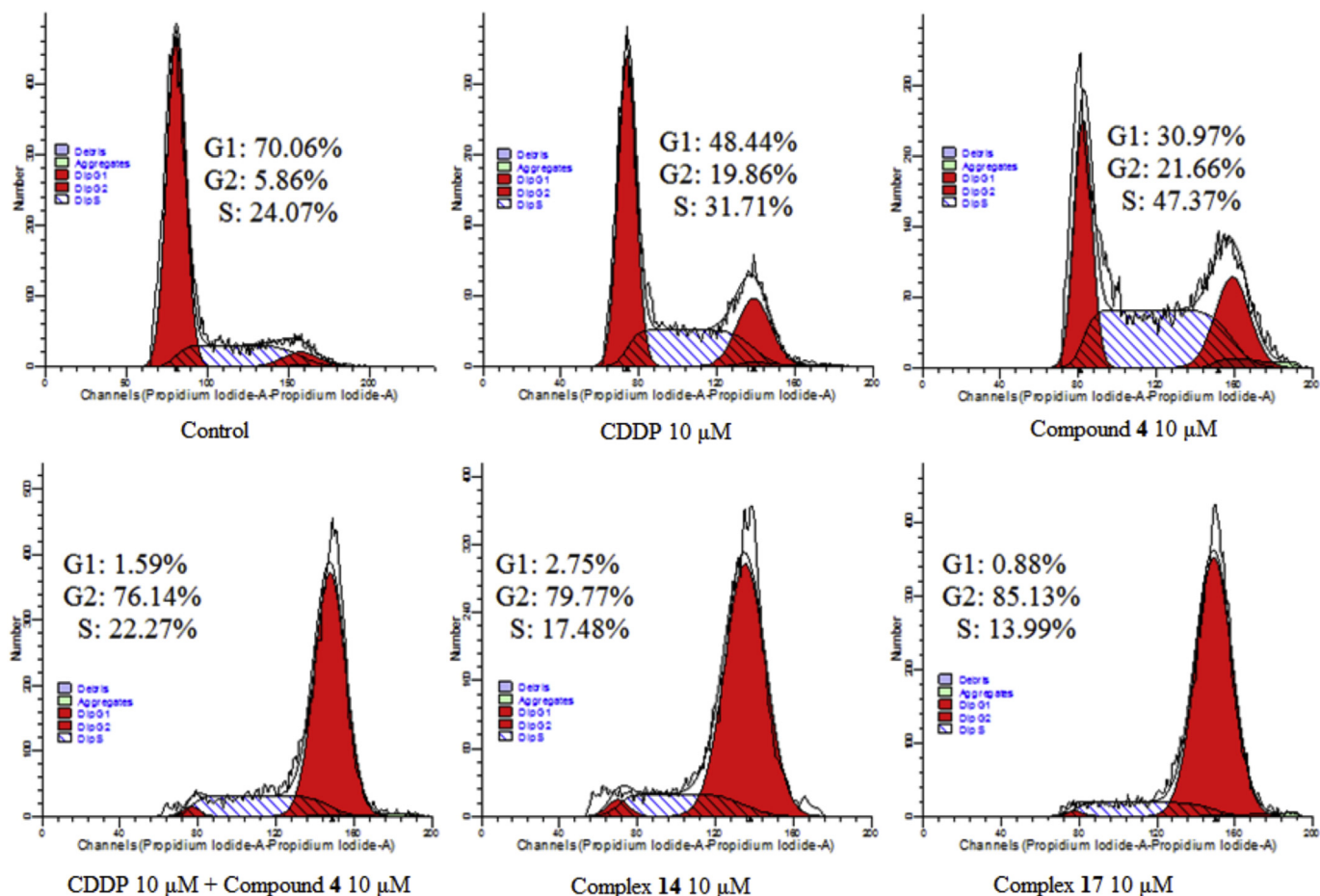


**Fig. 7.** Effects of Pt(IV) complexes **14** and **17** on cell cycle phase arrest in HepG-2 cells. Cells were treated with 10 μM of **14** and **17** for 48 h. Untreated cells were used as a negative control and cells treated with CDDP and **4** were used as positive controls for 48 h, respectively. Then the cells were fixed and stained with PI to analyze DNA content by flow cytometry. The experiments were performed three times, and the results of the representative experiments are shown.

spectrometer and far infrared spectra were obtained on a NEXUS870 FT-IR spectrometer.  $^1\text{H}$  NMR,  $^{13}\text{C}$  NMR and  $^{195}\text{Pt}$  NMR spectra were recorded in  $\text{CDCl}_3$  or  $\text{DMSO}-d_6$  with a Bruker 300, 400 or 600 MHz NMR spectrometer.

#### 4.1. General procedure for the preparation of compounds **14–16** and **17–19**

**Synthesis of compound 3.** An aqueous solution of 50% KOH (20 mL) was added dropwise to a stirred solution of 3',4',5'-trimethoxyacetophenone (**1**, 2.1 g, 10.0 mmol) and 4-methoxy-3-nitrobenzaldehyde (**2**, 1.8 g, 10.0 mmol) in methanol (35 mL) at 0 °C. The resulting mixture was stirred at the same temperature for overnight and monitored by TLC. After completion of reaction, the mixture was poured into water and adjusted to pH = 2 with 2 N HCl. The precipitated solid was filtered, washed with water and dried to offer the crude product which was purified by chromatography on silica gel eluted with petroleum ether/ethyl acetate (V:V = 4:1, 3:1, 2:1) to give the desired compound as a yellow solid (yield: 2.65 g, 71.0%).  $^1\text{H}$  NMR (300 MHz,  $\text{CDCl}_3$ )  $\delta$  8.17 (d,  $J$  = 2.0 Hz, 1H), 7.80–7.73 (m, 2H), 7.43 (d,  $J$  = 15.6 Hz, 1H), 7.28 (s, 2H), 7.15 (d,  $J$  = 8.8 Hz, 1H), 4.02 (s, 3H), 3.95 (d,  $J$  = 4.6 Hz, 9H).  $^{13}\text{C}$  NMR (100 MHz,  $\text{CDCl}_3$ )  $\delta$  188.42, 154.12, 153.22, 142.80, 141.62, 139.96, 134.50, 133.13, 127.64, 124.71, 121.95, 113.88, 106.17, 60.99, 56.79, 56.47. IR (KBr): 3451, 3065, 2996, 2952, 1653, 1577, 1530, 1457, 1414, 1353, 1276, 1161, 1128, 1002, 771  $\text{cm}^{-1}$ . Elemental analysis calcd (%)

for  $\text{C}_{19}\text{H}_{19}\text{NO}_7$ : C, 61.12; H, 5.13; N, 3.75; found: C, 61.23; H, 5.24; N, 3.51. HR-MS ( $m/z$ ) (ESI): calcd for  $\text{C}_{19}\text{H}_{19}\text{NO}_7$  [ $\text{M}+\text{H}^+$ ]: 374.12398; found: 374.11838.

**Synthesis of compound 4.** To a solution of compound **3** (1.86 g, 5.0 mmol) in ethanol (30 mL)/water (3 mL) was added iron powder (1.4 g, 25.00 mmol) and  $\text{NH}_4\text{Cl}$  (161 mg, 3.0 mmol). The reaction was stirred at 85 °C for 2 h and monitored by TLC. After completion of reaction, the mixture was cooled to room temperature and filtered through Celite. The filtered cake was washed with  $\text{CH}_2\text{Cl}_2$  (50 mL), and the filtrate was concentrated under pressure. The residue was dissolved in dichloromethane (50 mL), washed with water (100 mL), dried over anhydrous  $\text{Na}_2\text{SO}_4$  overnight, then the filtered solution was concentrated under pressure. The crude product was purified by chromatography on silica gel eluted with  $\text{CH}_2\text{Cl}_2/\text{MeOH}$  (V:V = 100:1) to give the desired compound as a yellow solid (yield: 1.6 g, 93.6%).  $^1\text{H}$  NMR (400 MHz,  $\text{CDCl}_3$ )  $\delta$  7.72 (d,  $J$  = 15.5 Hz, 1H), 7.30 (d,  $J$  = 15.9 Hz, 1H), 7.26 (s, 2H), 7.03 (d,  $J$  = 8.7 Hz, 2H), 6.80 (d,  $J$  = 7.9 Hz, 1H), 3.94 (d,  $J$  = 2.7 Hz, 9H), 3.89 (s, 3H).  $^{13}\text{C}$  NMR (100 MHz,  $\text{CDCl}_3$ )  $\delta$  189.42, 153.10, 149.72, 145.40, 142.21, 136.62, 133.96, 127.97, 121.02, 119.27, 113.29, 110.24, 106.00, 78.08, 77.41, 60.97, 56.39, 55.62. IR (KBr): 3444, 3358, 2939, 2834, 1650, 1575, 1510, 1461, 1411, 1345, 1265, 1153, 1124, 1025, 918, 788  $\text{cm}^{-1}$ . Elemental analysis calcd (%) for  $\text{C}_{19}\text{H}_{21}\text{NO}_5$ : C, 66.46; H, 6.16; N, 4.08; found: C, 66.35; H, 6.32; N, 3.91. HR-MS ( $m/z$ ) (ESI): calcd for  $\text{C}_{19}\text{H}_{21}\text{NO}_5$  [ $\text{M}+\text{H}^+$ ]: 344.14980; found: 344.14445.

**Synthesis of compounds 7 and 8.** To a solution of compound **5** or

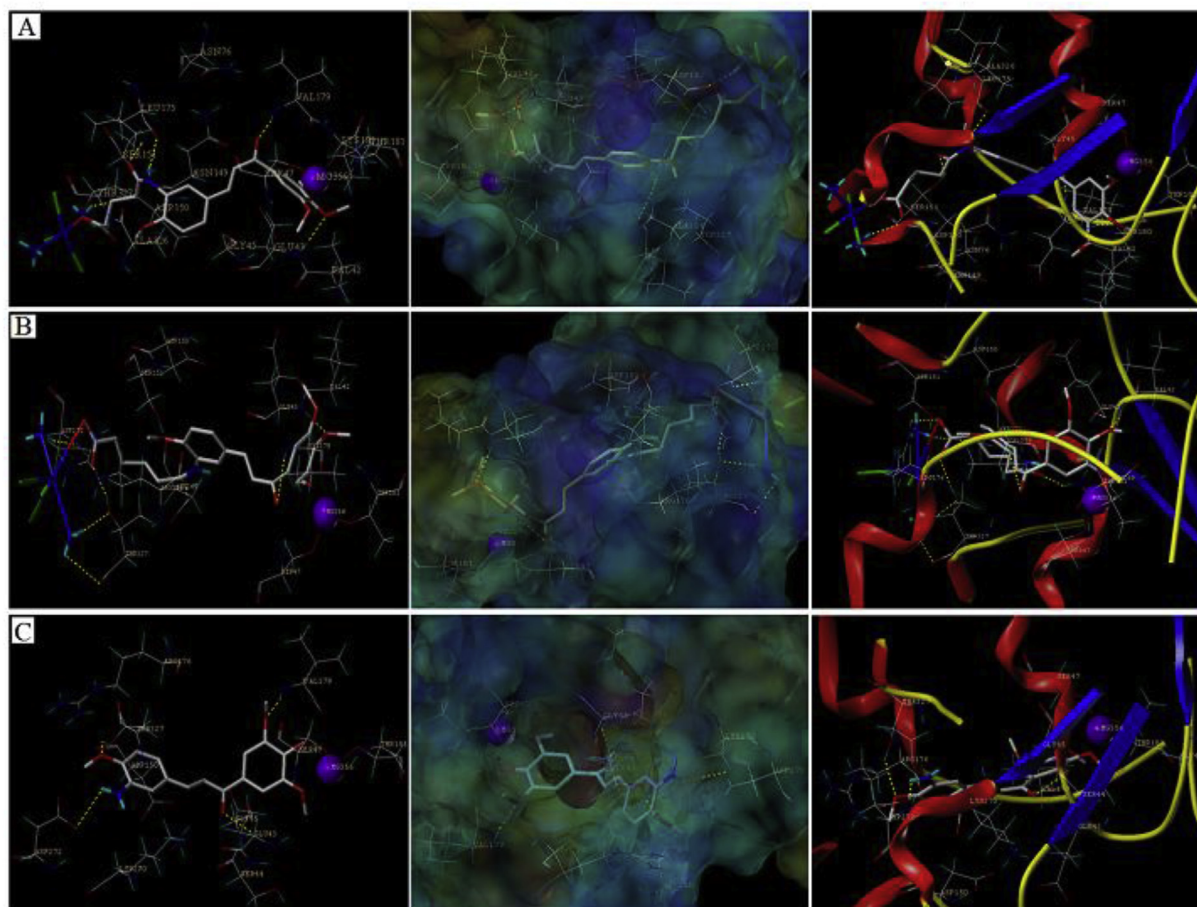


**Fig. 8.** Molecular modeling of **14**, **17** and **4** in complex with tubulin (PDB code: 1SA0ISA0). Illustrated are the proposed binding mode and interaction between tubulin and selected compounds, (A) compound **14**, (B) compound **17**, (C) compound **4**. The compounds and important amino acids in the binding pockets are shown in stick model, whereas tubulin is depicted in the ribbon model. The  $Mg^{2+}$ -ion is shown as a purple sphere.

**Table 4**  
Docking scores (kcal/mol) for all studied compounds.

Compd.	Score	Crash	Polar	D-Score	PMF-Score	G-Score	Chem-Score	CScore
<b>4</b>	6.59	−3.94	3.63	−127.595	−21.857	−245.693	−32.025	3
<b>14</b>	8.70	−9.15	6.54	−282.292	−12.206	−436.320	−39.748	3
<b>17</b>	11.11	−8.46	7.27	−249.353	−18.992	−443.562	−44.484	3

**6** (3.75 mmol) in dry  $CH_2Cl_2$  (30 mL) was added EDCI (959 mg, 5.0 mmol), DMAP (610 mg, 5.0 mmol) and compound **4** (860 mg, 2.5 mmol). The resulting mixture was stirred at room temperature for overnight and monitored by TLC. After completion of reaction, the mixture was diluted with  $CH_2Cl_2$  (100 mL) and washed with water (100 mL). The organic phase was dried over anhydrous  $Na_2SO_4$ , filtered, and concentrated under reduced pressure. The crude product which was purified by chromatography on silica gel eluted with petroleum ether/ethyl acetate (V:V = 5:1, 4:1, 3:1) to give compound **7** or **8**.

Compound **7**. 950 mg, 80.5% yield as a yellow solid.  $^1H$  NMR (300 MHz,  $CDCl_3$ )  $\delta$  8.81 (s, 1H), 7.81–7.74 (m, 2H), 7.39 (d,  $J = 15.6$  Hz, 1H), 7.30 (d,  $J = 8.5$  Hz, 1H), 7.27 (s, 2H), 6.91 (d,  $J = 8.5$  Hz, 1H), 3.95 (s, 6H), 3.94 (d,  $J = 2.9$  Hz, 6H), 3.69 (s, 3H), 2.53–2.45 (m, 4H), 2.13–2.03 (m, 2H).  $^{13}C$  NMR (100 MHz,  $CDCl_3$ )  $\delta$  189.43, 173.54, 170.59, 153.10, 149.70, 144.86, 142.30, 133.80, 128.15, 128.09, 125.81, 120.31, 118.43, 110.04, 106.10, 60.95, 56.43,

55.96, 51.63, 36.65, 32.96, 20.63. IR (KBr): 3443, 3292, 2944, 1731, 1656, 1581, 1541, 1494, 1462, 1438, 1413, 1351, 1309, 1268, 1157, 1130, 1071, 1021, 1005, 799  $cm^{-1}$ . Elemental analysis calcd (%) for  $C_{25}H_{29}NO_8$ : C, 63.68; H, 6.20; N, 2.97; found: C, 66.56; H, 6.39; N, 2.84. HR-MS ( $m/z$ ) (ESI): calcd for  $C_{25}H_{29}NO_8$  [ $M+H^+$ ]: 472.19714; found: 472.18732.

Compound **8**. 1.05 g, 86.8% yield as a yellow solid.  $^1H$  NMR (300 MHz,  $CDCl_3$ )  $\delta$  8.81 (s, 1H), 7.77 (d,  $J = 15.6$  Hz, 2H), 7.40 (d,  $J = 15.6$  Hz, 1H), 7.43–7.28 (m, 3H), 6.91 (d,  $J = 8.5$  Hz, 1H), 3.95 (s, 6H), 3.94 (d,  $J = 1.7$  Hz, 6H), 3.68 (s, 3H), 2.48–2.36 (m, 4H), 1.83–1.73 (m, 4H).  $^{13}C$  NMR (100 MHz,  $CDCl_3$ )  $\delta$  189.45, 173.80, 170.99, 153.10, 149.66, 144.88, 142.31, 133.81, 128.18, 128.11, 125.82, 120.31, 118.37, 110.01, 106.11, 60.95, 56.44, 55.96, 51.56, 37.54, 33.72, 24.95, 24.42. IR (KBr): 3422, 3311, 2944, 1735, 1660, 1581, 1533, 1493, 1441, 1415, 1344, 1263, 1159, 1125, 1071, 1025, 1001, 801  $cm^{-1}$ . Elemental analysis calcd (%) for  $C_{26}H_{31}NO_8$ : C, 64.32; H, 6.44; N, 2.88; found: C, 66.45; H, 6.57; N, 2.65. HR-MS ( $m/z$ ) (ESI): calcd for

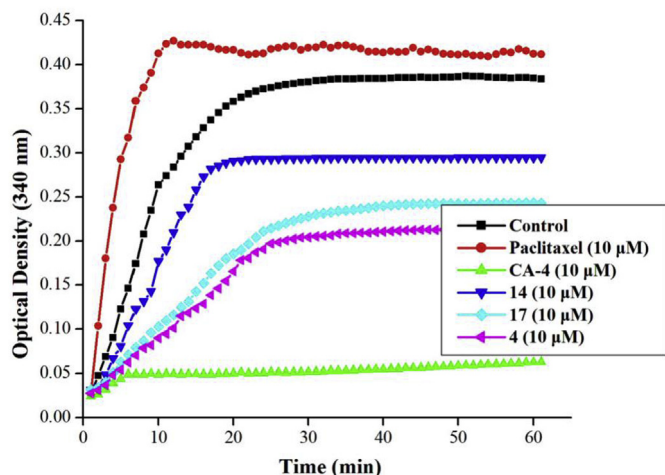


**Fig. 9.** Effects of complexes **14** and **17** on microtubule dynamics. Polymerization of tubulin at 37 °C in the presence of paclitaxel (10 μM), CA-4 (10 μM), **4** (10 μM), **14** (10 μM) and **17** (10 μM) were monitored continuously by recording the absorbance at 340 nm over 60 min. The reaction was initiated by the addition of tubulin to a final concentration of 3.0 mg/mL.

$C_{26}H_{31}NO_8$  [M+H<sup>+</sup>]: 486.21279; found: 486.20171.

**Synthesis of compounds 9 and 10.** To a solution of compound **7** (900 mg, 1.91 mmol) or **8** (925 mg, 1.91 mmol) in THF/H<sub>2</sub>O (30/5 mL) at 0 °C was added lithium hydroxide (241 mg, 5.73 mmol), the resulting mixture was stirred at the same temperature for 2 h. After completion of reaction, the mixture was adjusted to pH = 2 with 2 N HCl solution, then 100 mL of CH<sub>2</sub>Cl<sub>2</sub> was added and washed with water (100 mL). The organic phase was dried over anhydrous Na<sub>2</sub>SO<sub>4</sub> and concentrated under reduced pressure to obtain the target product.

**Compound 9.** 795 mg, 91.2% yield as a yellow solid. <sup>1</sup>H NMR (400 MHz, DMSO-*d*<sub>6</sub>) δ 11.90 (s, 1H), 9.27 (s, 1H), 8.26 (s, 1H), 7.76–7.65 (m, 3H), 7.40 (s, 2H), 7.14 (d, *J* = 8.6 Hz, 1H), 3.90 (d, *J* = 2.9 Hz, 9H), 3.77 (s, 3H), 2.43 (t, *J* = 7.3 Hz, 2H), 2.30 (t, *J* = 7.3 Hz, 2H), 1.85–1.79 (m, 2H). <sup>13</sup>C NMR (100 MHz, DMSO-*d*<sub>6</sub>) δ 188.35, 174.68, 171.63, 153.36, 152.92, 144.57, 142.31, 133.73, 128.00, 127.42, 126.63, 124.18, 120.34, 111.91, 106.58, 60.65, 56.67, 56.42, 35.55, 33.45, 21.05. IR (KBr): 3452, 3307, 2944, 1741, 1659, 1566, 1532, 1494, 1445, 1356, 1315, 1272, 1161, 1127, 1027, 1006, 767 cm<sup>-1</sup>. Elemental analysis calcd (%) for C<sub>24</sub>H<sub>27</sub>NO<sub>8</sub>: C, 63.01; H, 5.95; N, 3.06; found: C, 63.17; H, 6.09; N, 2.85. HR-MS (*m/z*) (ESI): calcd for C<sub>24</sub>H<sub>27</sub>NO<sub>8</sub> [M+H<sup>+</sup>]: 456.16584; found: 456.16883.

**Compound 10.** 850 mg, 94.4% yield as a yellow solid. <sup>1</sup>H NMR (300 MHz, DMSO-*d*<sub>6</sub>) δ 11.99 (s, 1H), 9.19 (s, 1H), 8.27 (s, 1H), 7.74–7.62 (m, 3H), 7.39 (s, 2H), 7.13 (d, *J* = 8.5 Hz, 1H), 3.90 (s, 9H), 3.77 (s, 3H), 2.39 (d, *J* = 6.1 Hz, 2H), 2.25 (t, *J* = 6.1 Hz, 2H), 1.67–1.49 (m, 4H). <sup>13</sup>C NMR (100 MHz, DMSO-*d*<sub>6</sub>) δ 188.35, 174.89, 171.94, 153.36, 152.82, 144.59, 142.31, 133.74, 128.07, 127.42, 126.51, 124.01, 120.33, 111.88, 106.57, 60.65, 56.67, 56.42, 36.13, 33.92, 25.19, 24.60. IR (KBr): 3421, 2939, 1725, 1656, 1583, 1534, 1502, 1461, 1341, 1310, 1263, 1158, 1126, 1024, 1000, 772 cm<sup>-1</sup>. Elemental analysis calcd (%) for C<sub>25</sub>H<sub>29</sub>NO<sub>8</sub>: C, 63.68; H, 6.20; N, 2.97; found: C, 63.81; H, 6.35; N, 2.74. HR-MS (*m/z*) (ESI): calcd for C<sub>25</sub>H<sub>29</sub>NO<sub>8</sub> [M+H<sup>+</sup>]: 470.118149; found: 470.22474.

**General synthesis of compounds 14–16.** To a solution of compound **9** (150 mg, 0.328 mmol), TBTU (158 mg, 0.492 mmol), and Et<sub>3</sub>N (50 mg, 0.492 mmol) in dry DMF (3 mL), compound **11**, **12**, or **13** (0.328 mmol) was added in portions and the mixture was stirred at room temperature for overnight. After completion of reaction, the whole mixture was added to CH<sub>2</sub>Cl<sub>2</sub> (150 mL), and then extracted twice with water (100 mL). The organic phase was dried

over anhydrous Na<sub>2</sub>SO<sub>4</sub> and concentrated under reduced pressure. The residue was purified on silica gel column eluted CH<sub>2</sub>Cl<sub>2</sub>/MeOH (V:V = 80:1, 60:1, 40:1) to give the desired product as a yellow solid.

**Compound 14.** 85 mg, 32.8% yield as a yellow solid. <sup>1</sup>H NMR (400 MHz, DMSO-*d*<sub>6</sub>) δ 9.12 (s, 1H), 8.29 (s, 1H), 7.76–7.63 (m, 3H), 7.39 (s, 2H), 7.12 (d, *J* = 8.6 Hz, 1H), 6.52–5.70 (m, 6H), 3.89 (s, 9H), 3.76 (s, 3H), 2.44–2.38 (m, 2H), 2.34–2.27 (m, 2H), 1.82–1.78 (m, 2H). <sup>13</sup>C NMR (100 MHz, DMSO-*d*<sub>6</sub>) δ 188.39, 180.61, 172.03, 153.35, 152.72, 144.64, 142.30, 133.72, 128.04, 127.39, 126.51, 123.75, 120.32, 111.89, 106.57, 60.67, 56.71, 56.49, 56.44, 36.08, 35.92, 22.25. <sup>195</sup>Pt NMR (129 MHz, DMSO-*d*<sub>6</sub>) δ 544.37. IR (KBr): 3422, 2923, 1641, 1582, 1530, 1485, 1417, 1338, 1287, 1260, 1070, 1025, 982, 800, 575, 527, 453, 344 cm<sup>-1</sup>. Elemental analysis calcd (%) for C<sub>24</sub>H<sub>32</sub>Cl<sub>3</sub>NO<sub>8</sub>Pt: C, 36.40; H, 4.07; N, 5.31; found: C, 36.53; H, 4.24; N, 5.12. HR-MS (*m/z*) (ESI): calcd for C<sub>24</sub>H<sub>32</sub>Cl<sub>3</sub>NO<sub>8</sub>Pt [M+H<sup>+</sup>]: 790.95900; found: 790.08831.

**Compound 15.** 135 mg, 47.4% yield as a yellow solid. <sup>1</sup>H NMR (400 MHz, DMSO-*d*<sub>6</sub>) δ 9.60–9.56 (m, 1H), 9.13 (s, 1H), 8.29 (s, 1H), 8.14 (s, 1H), 7.79 (s, 1H), 7.73–7.70 (m, 1H), 7.69–7.63 (m, 2H), 7.45 (d, *J* = 10.2 Hz, 1H), 7.38 (s, 2H), 7.12 (d, *J* = 8.7 Hz, 1H), 3.89 (s, 9H), 3.75 (s, 3H), 2.76–2.53 (m, 2H), 2.44 (t, *J* = 7.2 Hz, 2H), 2.33 (t, *J* = 7.4 Hz, 2H), 2.19–2.04 (m, 2H), 1.85–1.78 (m, 2H), 1.55–1.48 (m, 3H), 1.31–1.06 (m, 3H). <sup>13</sup>C NMR (100 MHz, DMSO-*d*<sub>6</sub>) δ 188.39, 183.23, 171.85, 153.35, 152.71, 144.62, 142.30, 133.72, 128.03, 127.40, 126.51, 123.77, 120.33, 111.90, 106.57, 63.86, 62.73, 60.67, 56.70, 56.48, 37.18, 35.80, 31.38, 31.33, 24.07, 24.03, 22.21. <sup>195</sup>Pt NMR (129 MHz, DMSO-*d*<sub>6</sub>) δ 412.86. IR (KBr): 3447, 3209, 2939, 1642, 1624, 1581, 1535, 1495, 1454, 1413, 1341, 1308, 1266, 1230, 1158, 1127, 1024, 808, 591, 537, 434, 347, 330 cm<sup>-1</sup>. Elemental analysis calcd (%) for C<sub>30</sub>H<sub>40</sub>Cl<sub>3</sub>N<sub>3</sub>O<sub>8</sub>Pt: C, 41.32; H, 4.62; N, 4.82; found: C, 41.21; H, 4.84; N, 4.63. HR-MS (*m/z*) (ESI): calcd for C<sub>30</sub>H<sub>40</sub>Cl<sub>3</sub>N<sub>3</sub>O<sub>8</sub>Pt [M+H<sup>+</sup>]: 869.14505; found: 870.16873.

**Compound 16.** 165 mg, 56.7% yield as a yellow solid. <sup>1</sup>H NMR (400 MHz, DMSO-*d*<sub>6</sub>) δ 9.19 (s, 1H), 8.54–8.26 (m, 4H), 7.74–7.63 (m, 4H), 7.39 (s, 2H), 7.12 (d, *J* = 8.6 Hz, 1H), 3.89 (d, *J* = 3.4 Hz, 9H), 3.76 (s, 3H), 2.59–2.50 (m, 2H), 2.40–2.34 (m, 4H), 2.11–2.01 (m, 2H), 1.80–1.74 (m, 2H), 1.55–1.37 (m, 4H), 1.25–1.10 (m, 2H). <sup>13</sup>C NMR (100 MHz, DMSO-*d*<sub>6</sub>) δ 188.39, 180.79, 171.78, 163.82, 153.36, 152.86, 144.62, 142.30, 133.72, 127.98, 127.39, 126.61, 124.02, 120.32, 111.94, 106.57, 62.03, 61.85, 60.67, 56.71, 56.45, 36.36, 35.66, 31.34, 31.05, 24.08, 24.00, 21.93. <sup>195</sup>Pt NMR (129 MHz, DMSO-*d*<sub>6</sub>) δ 1000.02. IR (KBr): 3450, 3416, 3201, 2945, 1722, 1655, 1584, 1536, 1500, 1456, 1416, 1350, 1257, 1221, 1154, 1125, 1025, 807, 571, 525, 456, 352, 321 cm<sup>-1</sup>. Elemental analysis calcd (%) for C<sub>32</sub>H<sub>40</sub>ClN<sub>3</sub>O<sub>12</sub>Pt: C, 43.22; H, 4.53; N, 4.73; found: C, 43.35; H, 4.67; N, 4.51. HR-MS (*m/z*) (ESI): calcd for C<sub>32</sub>H<sub>40</sub>ClN<sub>3</sub>O<sub>12</sub>Pt [M+H<sup>+</sup>]: 887.18700; found: 888.22014.

**General synthesis of compounds 17–19.** To a solution of compound **10** (150 mg, 0.318 mmol), TBTU (154 mg, 0.478 mmol), and Et<sub>3</sub>N (48 mg, 0.478 mmol) in dry DMF (3 mL), compound **11**, **12**, or **13** (0.318 mmol) was added in portions and the mixture was stirred at room temperature overnight. After completion of reaction, the whole mixture was added to CH<sub>2</sub>Cl<sub>2</sub> (150 mL), and then extracted twice with water (100 mL). The organic phase was dried over anhydrous Na<sub>2</sub>SO<sub>4</sub> and concentrated under reduced pressure. The residue was purified on silica gel column eluted CH<sub>2</sub>Cl<sub>2</sub>/MeOH (V:V = 80:1, 60:1, 40:1) to give the desired product as a yellow solid.

**Compound 17.** 65 mg, 25.4% yield as a yellow solid. <sup>1</sup>H NMR (400 MHz, DMSO-*d*<sub>6</sub>) δ 9.18 (s, 1H), 8.29 (s, 1H), 7.73–7.63 (m, 2H), 7.65 (d, *J* = 15.5 Hz, 1H), 7.38 (s, 2H), 7.12 (d, *J* = 8.7 Hz, 1H), 6.45–5.76 (m, 6H), 3.89 (d, *J* = 4.3 Hz, 9H), 3.76 (s, 3H), 2.40 (t, *J* = 6.8 Hz, 2H), 2.28 (t, *J* = 7.1 Hz, 2H), 1.65–1.51 (m, 4H). <sup>13</sup>C NMR (100 MHz, DMSO-*d*<sub>6</sub>) δ 188.39, 181.03, 174.90, 172.11, 153.36, 152.73, 144.65, 142.30, 133.73, 128.10, 127.38, 126.40, 123.86, 120.32, 111.91, 106.57, 60.67, 56.71, 56.49, 36.57, 36.25, 25.54, 25.29. <sup>195</sup>Pt NMR

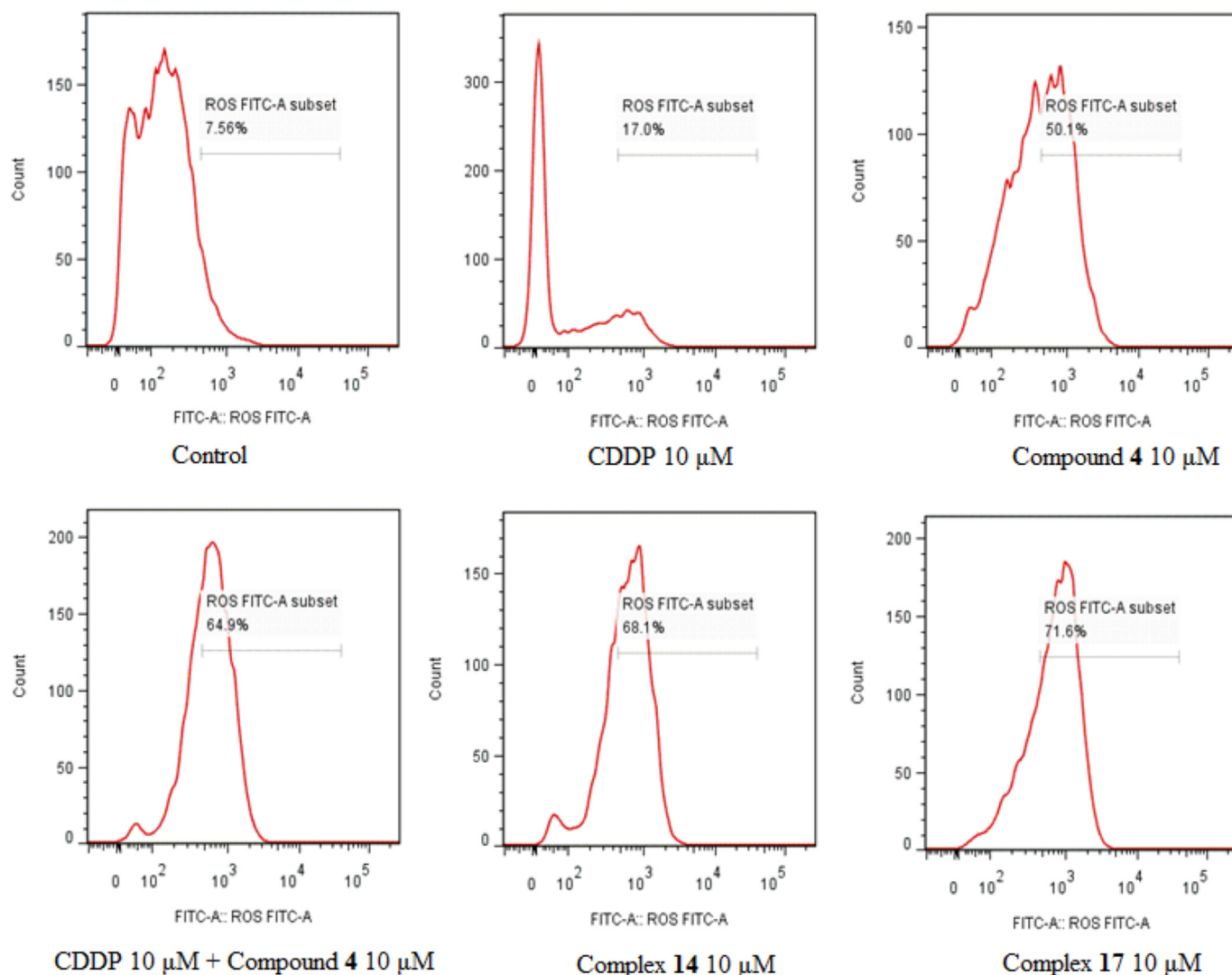


**Fig. 10.** Assessment of the ROS production in HepG-2 cells after 24 h incubations with **14** and **17**, cells were stained with DCF-DA and analyzed by flow cytometry. The experiments were performed three times, and the results of the representative experiments were shown.

(129 MHz, DMSO- $d_6$ )  $\delta$  544.67. IR (KBr): 3422, 3228, 2926, 1649, 1583, 1532, 1486, 1413, 1340, 1261, 1157, 1124, 988, 935, 808, 573, 529, 454, 344  $\text{cm}^{-1}$ . Elemental analysis calcd (%) for  $\text{C}_{25}\text{H}_{34}\text{Cl}_3\text{N}_3\text{O}_8\text{Pt}$ : C, 37.26; H, 4.25; N, 5.21; found: C, 37.38; H, 4.38; N, 5.01. HR-MS ( $m/z$ ) (ESI): calcd for  $\text{C}_{25}\text{H}_{34}\text{Cl}_3\text{N}_3\text{O}_8\text{Pt} [\text{M}+\text{Cl}^-]$ : 840.06971; found: 840.09689.

**Compound 18.** 145 mg, 51.6% yield as a yellow solid.  $^1\text{H}$  NMR (400 MHz, DMSO- $d_6$ )  $\delta$  9.62 (t,  $J=9.6$  Hz, 1H), 9.18 (s, 1H), 8.29 (s, 1H), 8.13 (s, 1H), 7.78 (s, 1H), 7.73–7.71 (m, 1H), 7.69–7.63 (m, 2H), 7.44 (d,  $J=10.3$  Hz, 1H), 7.38 (s, 2H), 7.12 (d,  $J=8.7$  Hz, 1H), 3.89 (s, 9H), 3.76 (s, 3H), 2.75–2.69 (m, 2H), 2.40 (d,  $J=6.7$  Hz, 2H), 2.29 (t,  $J=6.6$  Hz, 2H), 2.19–2.03 (m, 2H), 1.60–1.58 (m, 4H), 1.55–1.46 (m, 3H), 1.29–1.04 (m, 3H).  $^{13}\text{C}$  NMR (100 MHz, DMSO- $d_6$ )  $\delta$  188.39, 183.49, 172.06, 153.36, 152.69, 144.64, 142.30, 133.73, 128.07, 127.38, 126.39, 123.84, 120.32, 111.90, 106.57, 63.91, 62.67, 60.67, 56.70, 56.47, 37.58, 36.17, 31.41, 31.30, 25.56, 25.17, 24.08, 24.01.  $^{195}\text{Pt}$  NMR (129 MHz, DMSO- $d_6$ )  $\delta$  414.16. IR (KBr): 3423, 3197, 2932, 1650, 1583, 1532, 1502, 1486, 1453, 1413, 1340, 1262, 1158, 1126, 1022, 810, 574, 491, 438, 345  $\text{cm}^{-1}$ . Elemental analysis calcd (%) for  $\text{C}_{31}\text{H}_{42}\text{Cl}_3\text{N}_3\text{O}_8\text{Pt}$ : C, 42.02; H, 4.78; N, 4.74; found: C, 42.14; H, 4.90; N, 4.51. R-MS ( $m/z$ ) (ESI): calcd for  $\text{C}_{31}\text{H}_{42}\text{Cl}_3\text{N}_3\text{O}_8\text{Pt} [\text{M}-\text{H}^+]$ : 883.16070; found: 884.18738.

**Compound 19.** 135 mg, 47.2% yield as a yellow solid.  $^1\text{H}$  NMR (400 MHz, DMSO- $d_6$ )  $\delta$  9.20 (s, 1H), 8.55–8.50 (m, 1H), 8.32 (d,  $J=30.3$  Hz, 3H), 7.73–7.63 (m, 4H), 7.38 (s, 2H), 7.12 (d,  $J=8.7$  Hz, 1H), 3.89 (s, 9H), 3.76 (s, 3H), 2.61–2.50 (m, 2H), 2.37 (d,  $J=6.6$  Hz, 2H), 2.31 (t,  $J=6.4$  Hz, 2H), 2.12–2.01 (m, 2H), 1.55–1.47 (m, 4H), 1.45–1.35 (m, 4H), 1.21–1.01 (m, 2H).  $^{13}\text{C}$  NMR (100 MHz, DMSO- $d_6$ )  $\delta$  188.40, 181.43, 172.02, 163.69, 153.36, 152.76, 144.65, 142.30, 133.72, 128.05, 127.37, 126.45, 123.92, 120.30, 111.90, 106.56, 62.04, 61.94, 60.67, 56.69, 56.45, 36.81, 36.09, 31.39, 31.06, 25.45, 25.12, 24.07, 23.98.  $^{195}\text{Pt}$  NMR (129 MHz, DMSO- $d_6$ )  $\delta$  996.61. IR (KBr): 3423, 3179, 2937, 1728, 1657, 1582, 1534, 1502, 1487, 1453, 1414, 1342, 1262, 1157, 1126, 1023, 806, 574, 455, 358, 321  $\text{cm}^{-1}$ . Elemental analysis calcd (%) for  $\text{C}_{33}\text{H}_{42}\text{Cl}_3\text{N}_3\text{O}_{12}\text{Pt}$ : C, 43.88; H, 4.69; N, 4.65; found: C, 43.76; H, 4.89; N, 4.46. HR-MS ( $m/z$ ) (ESI): calcd for  $\text{C}_{33}\text{H}_{42}\text{Cl}_3\text{N}_3\text{O}_{12}\text{Pt} [\text{M}-\text{H}^+]$ : 902.23400; found: 902.23301.

#### 4.2. Cell culture and maintenance

All human cancer cell lines and two human normal cell lines in this study were purchased from China Life Science Collage (Shanghai, PRC). Culture medium Dulbecco's modified Eagle medium (DMEM), fetal bovine serum (FBS), phosphate buffered saline

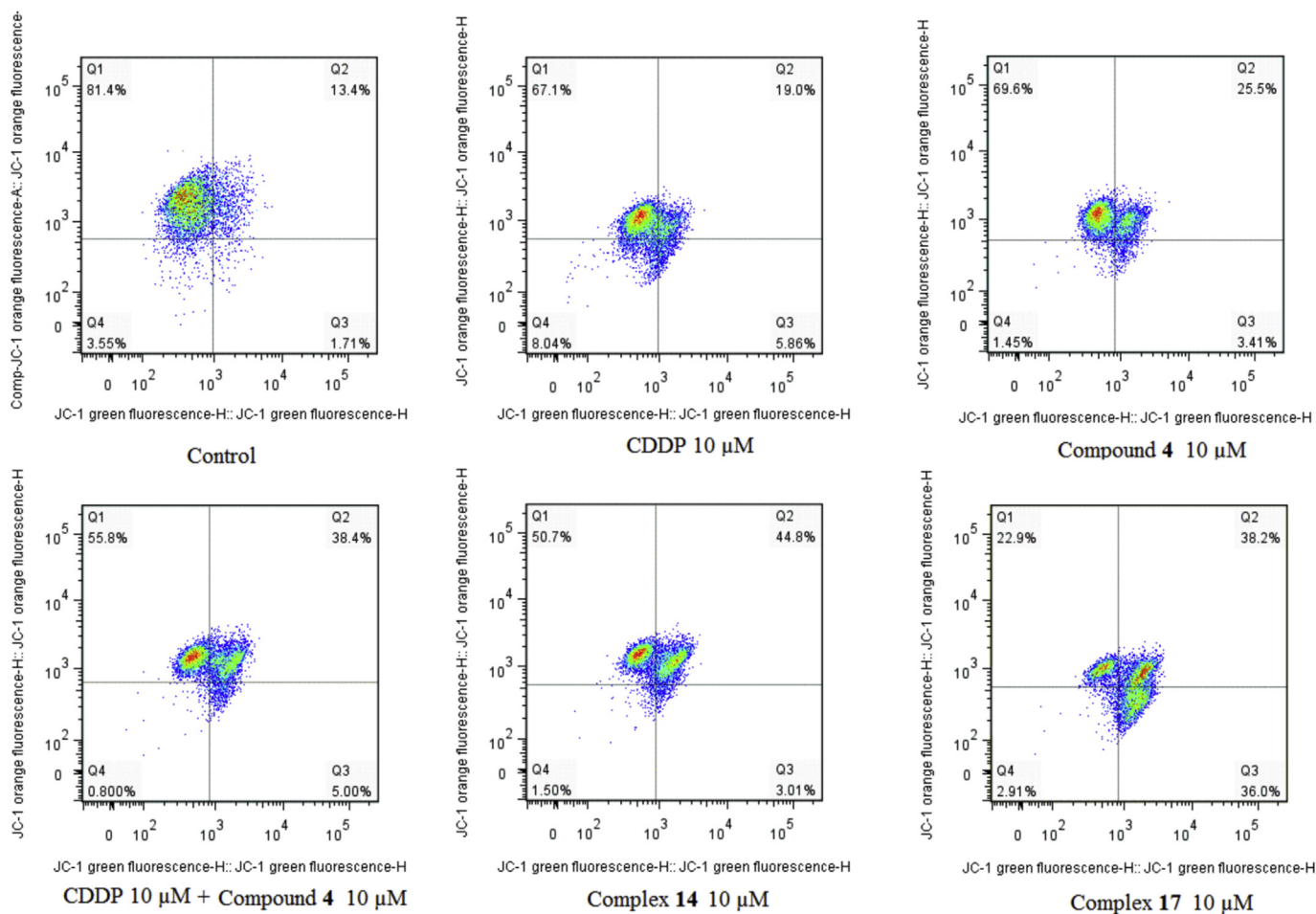


**Fig. 11.** Complexes **14** and **17** decreased the MMP of HepG-2 cells. The HepG-2 cells were treated with **14** and **17** at the indicated concentration for 24 h followed by incubation with the fluorescence probe JC-1 for 30 min, and then the cells were detected by flow cytometry. The experiments were performed three times, and the results of the representative experiments were shown.

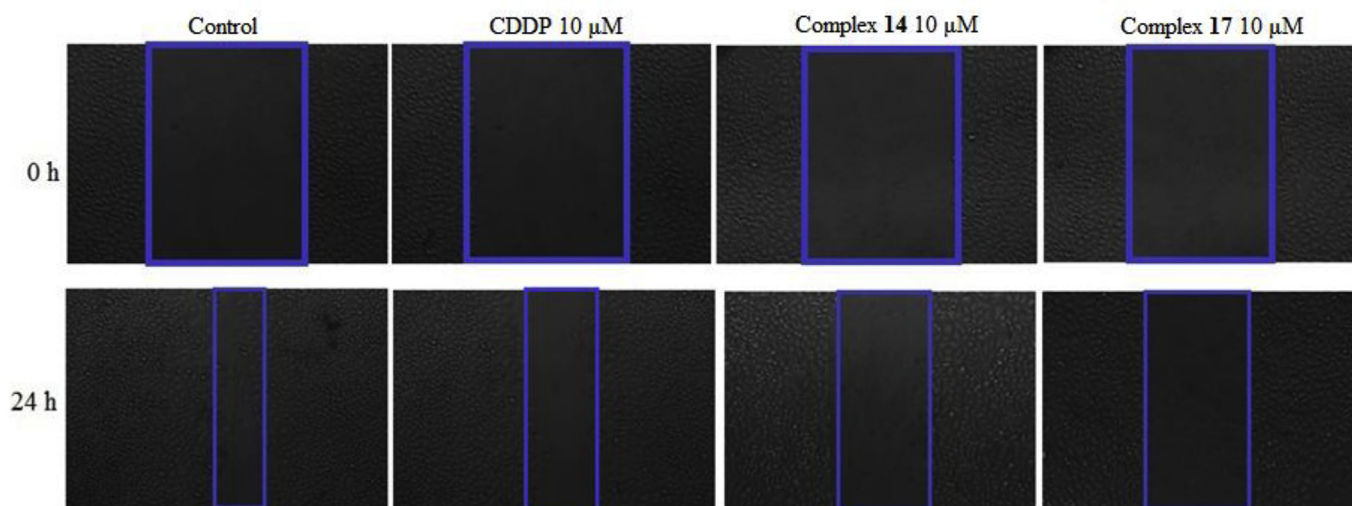


**Fig. 12.** Complexes **14** and **17** inhibited the migration of HUVEC cells *in vitro*. At the same concentration of CDDP, complexes **14** and **17** suppressed HUVEC cells migration. The experiments were performed three times, and the results of the representative experiments were shown.

(PBS, pH = 7.2), and Antibiotic-Antimycotic came from KeyGen Biotech Company (China). Cell lines were grown in the

supplemented with 10% FBS, 100 units/ml of penicillin and 100 g/ml of streptomycin in a humidified atmosphere of 5% CO<sub>2</sub> at 37 °C.

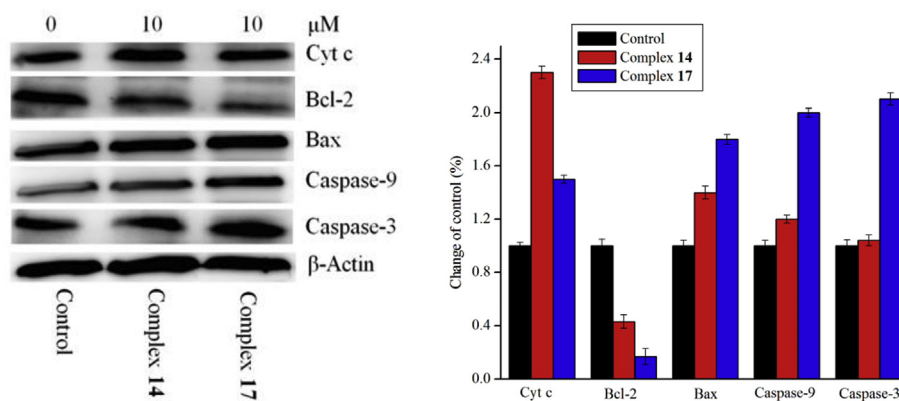


**Fig. 13.** Western blot analysis of Cyt c, Bax, Bcl-2, caspase-9 and caspase-3 after treatment of HepG-2 cells with **14** and **17** at the indicated concentration for 48 h.  $\beta$ -Actin antibody was used as reference control. The experiments were performed three times, and the results of the representative experiments were shown.

#### 4.3. Cytotoxicity assay

The anticancer activity of the title compounds were dissolved in DMF and evaluated in three human cancer cells (HepG-2, SK-OV-3 and NCI-H460) and two human normal cells (HL-7702 and BEAS-2B) and CDDP-resistance cells (A549/CDDP), respectively. About  $1.0 \times 10^5$  cells/mL cells, which were in the logarithmic phase, were grown in each well of 96-well plates and incubated for 12 h at 37 °C in 5% CO<sub>2</sub>. Complexes at five different concentrations (2.5, 5, 10, 20 and 50  $\mu$ M) were also added to the test well and then the cells were incubated at 37 °C in a 5% CO<sub>2</sub> atmosphere for 72 h. An enzyme labeling instrument was used to read absorbance with 570/630 nm double wavelength measurement. Cytotoxicity was detected on the percentage of cell survival compared with the negative control. The final IC<sub>50</sub> values were calculated by the Bliss method ( $n = 5$ ). All of the tests were repeated in triplicate.

#### 4.4. Cell uptake

HepG-2 cells were grown in each well of 96-well plates. After the cells reached about 80% confluence, 10 and 20  $\mu$ M of CDDP, **14** and **17** were added and the plates were also incubated for 24 h at 37 °C in 5% CO<sub>2</sub>, respectively. After completion of 24 h incubation, cells were collected and washed three times with ice-cold PBS, then centrifuged at  $1000 \times g$  for 10 min and resuspended in 2 mL PBS. A volume of 100  $\mu$ L was taken out to examine the cell density. The remaining cells were digested by HNO<sub>3</sub> (200  $\mu$ L, 65%) at 65 °C for 12 h. The Pt level in cells were detected by ICP-MS.

#### 4.5. Molecular docking

All the docking studies were carried out using Sybyl-X 2.0 on a windows workstation. The crystal structure of the tubulin in complex with colchicine was retrieved from the RCSB Protein Data Bank (PDB:1SA0.pdb) [50]. The synthetic chalcone analogues, Pt(IV) complexes (**14** and **17**) including the parent compound **4**, were selected for the docking studies. The 3D structures of these selected compounds were first built using Sybyl-X 2.0 sketch followed by energy minimization using the MMFF94 force field and Gasteiger-Marsili charges. We employed Powell's method for optimizing the geometry with a distance dependent dielectric constant and a termination energy gradient of 0.005 kcal/mol. All the selected compounds were automatically docked into the colchicine binding pocket of tubulin by an empirical scoring function and a patented search engine in the Surflex docking program. Before the docking process, the natural ligand was extracted; the water molecules

were removed from the crystal structure. Subsequently, the protein was prepared by using the Biopolymer module implemented in Sybyl. The polar hydrogen atoms were added. The automated docking manner was applied in the present work. Other parameters were established by default to estimate the binding affinity characterized by the Surflex-Dock scores in the software. Surflex-Dock total scores, which were expressed in  $-\log_{10}$  (Kd) units to represent binding affinities, were applied to estimate the ligand-receptor interactions of newly designed molecules. A higher score represents stronger binding affinity. The optimal binding pose of the docked compounds was selected based on the Surflex scores and visual inspection of the docked complexes.

#### 4.6. Flow cytometry analysis of cell cycle distribution

HepG-2 cells were grown on 6-well plates and treated with **4**, CDDP, **14**, **17** and CDDP/**4** at the same concentrations (10  $\mu$ M) and maintained with of the proper culture medium in 5% CO<sub>2</sub> at 37 °C for 48 h. After completion of incubation, cells were harvested and washed three times with ice-cold PBS, fixed with ice-cold 70% ethanol at  $-20$  °C for overnight. The cells were treated with 100  $\mu$ g/mL RNase A for 30 min at 37 °C after washed with twice ice-cold PBS, and finally stained with 1 mg/mL propidium iodide (PI) in the dark at 4 °C for 30 min. Analysis was performed with the system software (Cell Quest; BD Biosciences).

#### 4.7. Apoptosis analysis

Apoptosis was also evaluated by flow cytometric analysis of annexin V/PI staining. HepG-2 cells were grown in each well of six-well plates at the density of  $5.0 \times 10^4$  cells/mL of the DMEM medium with 10% FBS to the final volume of 2 mL. The plates were incubated for overnight and treated with **4**, CDDP, **14**, **17** and CDDP/**4** at the same concentration (10  $\mu$ M) for 24 h. Briefly, cells were harvested and washed with twice ice-cold PBS, and then suspended cells in the annexin-binding buffer at a concentration of  $5 \times 10^5$  cells/ml. cells were then incubated with 5  $\mu$ L of annexin V-FITC and 5  $\mu$ L of PI in the dark at 4 °C for 30 min. The cells were detected by system software (Cell Quest; BD Biosciences).

#### 4.8. AO/EB double staining

HepG-2 cells were grown in each well of six-well plates at the density of  $5.0 \times 10^4$  cells/mL of the DMEM medium with 10% FBS to the final volume of 2 mL. The plates were incubated for overnight and treated with **4**, CDDP, **14**, **17** and CDDP/**4** at the same

concentration (10  $\mu$ M) for 24 h. After the treatment period, the cover slip with monolayer cells were inverted on a glass slide with 20  $\mu$ L of AO/EB stain (100 mg/mL). Fluorescence was read on a Nikon ECLIPSETE2000-S fluorescence microscope (OLYMPUS Co., Japan).

#### 4.9. Mitochondrial membrane potential (MMP) assay

The MMP was measured with the lipophilic cation probe JC-1 (Beyotime, Haimen, China, Molecular Probe), as previously described [51]. HepG-2 cells were seeded into six-well plates and treated with the same concentration (10  $\mu$ M) of the test compounds for 24 h. After incubation for 24 h, the JC-1 fluorescent probe was added 20 min after replacing with fresh medium. Cells were collected at 2500 rpm and washed twice with ice-cold PBS and then the MMP were examined by flow cytometer, respectively. The emission fluorescence for JC-1 was detected by 530 and 590 nm, under the excitation wavelength at 488 nm, respectively.

#### 4.10. ROS assay

The production of ROS was examined by flow cytometry using DCFH-DA (Molecular Probe, Beyotime, Haimen, China), as previously described [45,51]. HepG-2 cells were grown into six-well plates and treated with the same concentration (10  $\mu$ M) of the test compounds for 24 h. On the following treatment, cells were harvested at 2000 rpm and washed twice with ice-cold PBS, and then resuspend cells in 10 mM DCFH-DA dissolved in cell free medium at 37 °C for 30 min in dark, and then washed twice with PBS. Cellular fluorescence was detected by flow cytometry at an excitation of 485 nm and an emission of 538 nm, respectively.

#### 4.11. Migration assay

The migration effects of complexes **14** and **17** on HUVEC cells were detected by wound-heal assay. HUVEC cells were grown into six-well plates and treated with at the same concentration (10  $\mu$ M) of the test complexes **14** and **17** for 24 h, respectively. The extent of wound heal was observed after 24 h by imaging with fluorescence microscope.

#### 4.12. Western blot analysis

Western blot analysis was performed as described previously [45,51]. HepG-2 cells were treated with the same concentration (10  $\mu$ M) of the test complexes **14** and **17** for 48 h, respectively. After incubation for 48 h, cells were collected, centrifuged, and washed twice with ice-cold PBS. The pellet was then resuspended in lysis buffer. After the cells were lysed on ice for 30 min, lysates were centrifuged at 20000 g at 4 °C for 5 min. The protein concentration in the supernatant was examined using the BCA protein assay reagents (Imgenex, USA). Equal amounts of protein per line were separated on 12% SDS polyacrylamide gel electrophoresis and transferred to PVDF Hybond-P membrane (GE Healthcare). Membranes were incubated with 5% skim milk in Tris-buffered saline with Tween 20 (TBST) buffer for 1 h and then the membranes being gently rotated overnight at 4 °C. Membranes were then incubated with primary antibodies against Bcl-2, Bax, Cyt c, caspase-9, caspase-3 or  $\beta$ -actin for overnight at 4 °C. Membranes were next incubated with peroxidase labeled secondary anti-bodies for 2 h, and then all membranes were washed with TBST three times for 15 min and the protein blots were detected with chemiluminescence reagent (Thermo Fischer Scientifics Ltd.). The X-ray films were developed with developer and fixed with fixer solution.

#### 4.13. Tubulin polymerization assay in vitro

Tubulin polymerization assay was monitored by the change in optical density at 340 nm using a modification of methods described by Jordan et al. [28] Purified brain tubulin polymerization kit was purchased from Cytoskeleton (BK006P, Denver, CO). The final buffer concentrations for tubulin polymerization contained 80.0 mM piperazine-*N,N'*-bis(2-ethanesulfonic acid) sequeisodium salt (pH 6.9), 2.0 mM MgCl<sub>2</sub>, 0.5 mM ethylene glycol bis( $\beta$ -aminoethyl ether)-*N,N,N',N'*-tetraacetic acid (EGTA), 1 mM GTP, and 10.2% glycerol. Test compounds were added at the indicated concentration (10  $\mu$ M), and then all components except the purified tubulin were warmed to 37 °C. The reaction was initiated by the addition of tubulin to a final concentration of 3.0 mg/mL. Paclitaxel, CA-4 and compound **4** were used as positive controls under similar experimental conditions. The optical density was measured for 1 h at 1 min intervals in BioTek's Synergy 4 multifunction microplate spectrophotometer with a temperature controlled cuvette holder. Assays were performed according to the manufacturer's instructions and under conditions similar to those employed for the tubulin polymerization assays described above [52,53].

#### 4.14. Statistical analysis

All statistical analysis was performed with SPSS Version 10. Data was analyzed by one-way ANOVA. Mean separations were performed using the least significant difference method. Each experiment was replicated thrice, and all experiments yielded similar results. Measurements from all the replicates were combined, and treatment effects were analyzed.

#### Acknowledgments

We are grateful to the National Natural Science Foundation of China (Grant No. 21571033) and the New Drug Creation Project of the National Science and Technology Major Foundation of China (Grant No. 2015ZX09101032) for financial aids to this work. The authors would also like to thank the Fundamental Research Funds for the Central Universities (Project 2242016K30020) for supplying basic facilities to our key laboratory. We also want to express our gratitude to the Priority Academic Program Development of Jiangsu Higher Education Institutions for the construction of fundamental facilities (Project 1107047002). Huang is grateful to the Innovation Program of Jiangsu Province postgraduate education (Project KYLX16\_0263). The research was also supported by the Scientific Research Foundation of Graduated School of Southeast University (YBJJ1677).

#### Appendix A. Supplementary data

Supplementary data related to this article can be found at <https://doi.org/10.1016/j.ejmech.2018.01.075>.

#### References

- [1] V. Pinzani, F. Bressolle, I.J. Haug, M. Galtier, J.P. Blayac, P. Balmes, Cisplatin-induced renal toxicity and toxicity-modulating strategies: a review, *Canc. Chemother. Pharmacol.* 35 (1994) 1–9.
- [2] N.J. Wheate, S. Walker, G.E. Craig, R. Oun, The status of platinum anticancer drugs in the clinic and in clinical trials, *Dalton Trans.* 39 (2010) 8113–8127.
- [3] E. Cvitkovic, M. Bekradda, Oxaliplatin: a new therapeutic option in colorectal cancer, *Semin. Oncol.* 26 (1999) 647–662.
- [4] N. Graf, S.J. Lippard, Redox Activation of metal-based pro-drugs as a strategy for drug delivery, *Adv. Drug Deliv. Rev.* 64 (2012) 993–1004.
- [5] F.F. Liu, S.H. Gou, F.H. Chen, L. Fang, J. Zhao, Study on antitumor platinum(II) complexes of chiral diamines with dicyclic species as steric hindrance, *J. Med. Chem.* 58 (2015) 6368–6377.
- [6] S. Piccinonna, N. Margiotta, C. Pacifico, Denora, A. Lopalco, N.S. Fedi,

- M. Corsinic, G. Natile, Dinuclear Pt(II)-bisphosphonate complexes: a scaffold for multinuclear or different oxidation state platinum drugs, *Dalton Trans.* 41 (2012) 9689–9699.
- [7] J.J. Wilson, S.J. Lippard, *In vitro* Anticancer Activity of cis-diammineplatinum(II) complexes with  $\beta$ -diketonate leaving group ligands, *J. Med. Chem.* 55 (2012) 5326–5336.
- [8] H.Y. Yu, S.H. Gou, Z.M. Wang, F.H. Chen, L. Fang, Toward overcoming cisplatin resistance via sterically hindered platinum(II) complexes, *Eur. J. Med. Chem.* 114 (2016) 141–152.
- [9] H.Y. Zhang, S.H. Gou, J. Zhao, F.H. Chen, G. Xu, X. Liu, Cytotoxicity profile of novel sterically hindered platinum(II) complexes with (1R,2R)-N<sup>1</sup>, N<sup>2</sup>-dibutyl-1, 2-diaminocyclohexane, *Eur. J. Med. Chem.* 96 (2015) 187–195.
- [10] X. Wang, Z.J. Guo, Targeting and delivery of platinum-based anticancer drugs, *Chem. Soc. Rev.* 42 (2013) 202–224.
- [11] X.P. Han, J. Sun, Y.J. Wang, Z.G. He, Recent advances in platinum(IV) complex-based delivery systems to improve platinum (II) anticancer therapy, *Med. Res. Rev.* 35 (2015) 1268–1299.
- [12] L. Kelland, The Resurgence of platinum-based cancer chemotherapy, *Nat. Rev. Canc.* 7 (2007) 573–584.
- [13] Y. Song, K. Suntharalingam, J.S. Yeung, M. Royzen, S.J. Lippard, Synthesis and characterization of Pt(IV) fluoroscein conjugates to investigate Pt(IV) intracellular transformations, *J. Inorg. Biochem.* 24 (2013) 1733–1740.
- [14] X.C. Huang, R.Z. Huang, S.H. Gou, Z.M. Wang, Z.X. Liao, H.S. Wang, Anticancer platinum(IV) prodrugs containing monoaminophosphonate ester as a targeting group inhibit matrix metalloproteinases and reverse multidrug resistance, *Bioconjugate Chem.* 28 (2017) 1305–1323.
- [15] X. Xue, S. You, Q. Zhang, Yan Wu, G.Z. Zou, P.C. Wang, Y.L. Zhao, Y. Xu, L. Jia, X.N. Zhang, X.J. Liang, Mitaplatin increases sensitivity of tumor cells to cisplatin by inducing mitochondrial dysfunction, *Mol. Pharm.* 9 (2012) 634–644.
- [16] R.K. Pathak, S. Marrache, J.H. Choi, T.B. Berding, S. Dhar, The Pro-drug platinum-A: simultaneous release of cisplatin and aspirin, *Angew. Chem. Int. Ed.* 53 (2014) 1963–1967.
- [17] R. Raveendran, J.P. Braude, E. Wexselblatt, V. Novohradsky, O. Stuchlikova, V. Brabec, V. Gandin, D. Gibson, Pt(IV) Derivatives of cisplatin and oxaliplatin with phenylbutyrate axial ligands are potent cytotoxic agents that act by several mechanisms of action, *Chem. Sci.* 7 (2016) 2381–2391.
- [18] X.C. Huang, R.Z. Huang, S.H. Gou, Z.M. Wang, Z.X. Liao, H.S. Wang, Combretastatin A-4 analogue: a dual-targeting and tubulin inhibitor containing antitumor Pt(IV) moiety with a unique mode of action, *Bioconjugate Chem.* 27 (2016) 2132–2148.
- [19] F.H. Chen, X.C. Huang, M. Wu, S.H. Gou, W.W. Hu, A CK2-targeted Pt(IV) prodrug to disrupt DNA damage response, *Canc. Lett.* 385 (2017) 168–178.
- [20] J. Seligmann, C. Twelves, Tubulin: an example of targeted chemotherapy, *Future Med. Chem.* 5 (2013) 339–352.
- [21] M. Kavallaris, Microtubules and resistance to tubulin-binding agents, *Nat. Rev. Cancer* 10 (2010) 194–204.
- [22] Y.V. Voitovich, E.S. Shegravina, N.S. Sitnikov, V.I. Faerman, V.V. Fokin, H.G. Schmalz, S. Combes, D. Allegro, P. Barbier, I.P. Beletskaya, E.V. Svirshchevskaya, A.Y. Fedorov, Synthesis and biological evaluation of furanoloalcolchicinoids, *J. Med. Chem.* 58 (2015) 692–704.
- [23] R.A. Stanton, K.M. Gernert, J.H. Nettles, R. Aneja, Drugs that target dynamic microtubules: a new molecular perspective, *Med. Res. Rev.* 31 (2011) 443–481.
- [24] R. Romagnoli, P.G. Baraldi, M.K. Salvador, D. Preti, M.A. Tabrizi, A. Brancale, X.H. Fu, J. Li, S.Z. Zhang, E. Hamel, R. Bortolozzi, E. Porcú, G. Basso, G. Viola, Discovery and optimization of a series of 2-Aryl-4-Amino-5-(3',4',5'-trime-thoxybenzoyl) thiazoles as novel anticancer agents, *J. Med. Chem.* 55 (2012) 5433–5445.
- [25] P.B. Schiff, J. Fant, S.B. Horwitz, Promotion of microtubule assembly *in vitro* by taxol, *Nature* 277 (1979) 665–667.
- [26] B. Gigant, C. Wang, R.B. Ravelli, F. Roussi, M.O. Steinmetz, P.A. Curmi, A. Sobel, M. Knossow, Structural basis for the regulation of tubulin by vinblastine, *Nature* 435 (2005) 519–522.
- [27] J. Löwe, H. Li, K.H. Downing, E. Nogales, Refined structure of  $\alpha$ ,  $\beta$ -tubulin at 3.5 Å resolution, *J. Mol. Biol.* 313 (2001) 1045–1057.
- [28] M.A. Jordan, L. Wilson, Microtubules as a target for anticancer drugs, *Nat. Rev. Canc.* 4 (2004) 253–265.
- [29] G.C. Wang, C.Y. Li, L. He, K. Lei, F. Wang, Y.Z. Pu, Z. Yang, D. Cao, L. Ma, J.Y. Chen, Y. Sang, X.L. Liang, M.L. Xiang, A.H. Peng, Y.Q. Wei, L.J. Chen, Design, synthesis and biological evaluation of a series of pyranochalcone derivatives containing indole moiety as novel anti-tubulin agents, *Bioorg. Med. Chem.* 22 (2014) 2060–2079.
- [30] V. Peyrot, C. Briand, R. Momburg, J.C. Sari, *In vitro* mechanism study of microtubule assembly inhibition by cis-dichlorodiammine-platinum (II), *Biochem. Pharmacol.* 35 (1986) 371–375.
- [31] Z. Yang, W. Wu, J. Wang, L. Liu, L. Li, J. Yang, G. Wang, D. Cao, R. Zhang, M. Tang, J. Wen, J. Zhu, W. Xiang, F. Wang, L. Ma, M. Xiang, J. You, L.J. Chen, Synthesis and biological evaluation of novel millepachine derivatives as a new class of tubulin polymerization inhibitors, *J. Med. Chem.* 57 (2014) 7977–7989.
- [32] J. Yan, J. Chen, S. Zhang, J.H. Hu, L. Huang, X.S. Li, Synthesis, evaluation, and mechanism study of novel indolechalcone derivatives exerting effective antitumor activity through microtubule destabilization *in vitro* and *in vivo*, *J. Med. Chem.* 59 (2016) 5264–5283.
- [33] J. Chen, J. Yan, J. Hu, Y. Pang, L. Huang, X. Li, Synthesis, biological evaluation and mechanism study of chalcone analogues as novel anti-cancer agents, *RSC Adv.* 5 (2015) 68128–68135.
- [34] D. Kumar, N.M. Kumar, K. Akamatsu, E. Kusaka, H. Harada, T. Ito, Synthesis and biological evaluation of indolychalcones as antitumor agents, *Bioorg. Med. Chem. Lett* 20 (2010) 3916–3919.
- [35] M.L. Edwards, D.M. Stemerick, P.S. Sunkara, Chalcones: a new class of anti-mitotic agents, *J. Med. Chem.* 133 (1990) 1948–1954.
- [36] S. Ducki, D. Rennison, M. Woo, A. Kendall, J.F.D. Chabert, A.T. McGown, N.J. Lawrence, Combretastatin-like chalcones as inhibitors of microtubule polymerization. Part 1: synthesis and biological evaluation of anti-vascular activity, *Bioorg. Med. Chem.* 17 (2009) 7698–7710.
- [37] S. Tuncel, A. Trivella, D. Atilla, K. Bennis, H. Savoie, F. Albrieux, L. Delort, H. Billard, V. Dubois, V. Ahsen, F.C. Chézet, C. Richard, R.W. Boyle, S. Ducki, F. Dumoulin, Assessing the dual activity of a chalcone-phthalocyanine conjugate: design, synthesis, and anti-vascular and photodynamic properties, *Mol. Pharm.* 10 (2013) 3706–3716.
- [38] S. Ducki, D. Rennison, M. Woo, A. Kendall, J.F.D. Chabert, A.T. McGown, N.J. Lawrence, Combretastatin-like chalcones as inhibitors of microtubule polymerization. Part 1: synthesis and biological evaluation of anti-vascular activity, *Bioorg. Med. Chem.* 17 (2009) 7698–7710.
- [39] R. Schobert, B. Biersack, A. Dietrich, S. Knauer, M. Zoldakova, A. Fruehauf, T. Mueller, Pt (II) complexes of a combretastatin A-4 analog chalcone: effects of conjugation on cytotoxicity, tumor specificity, and long-term tumor growth suppression, *J. Med. Chem.* 52 (2009) 241–246.
- [40] M. Ravera, E. Gabano, G. Pelosi, F. Fregonese, S. Tinello, D. Osella, A new entry to asymmetric platinum(IV) complexes via oxidative chlorination, *Inorg. Chem.* 53 (2014) 9326–9335.
- [41] Y. Gou, J. Wang, S.F. Chen, Z. Zhang, Y. Zhang, W. Zhang, F. Yang, a-N-heterocyclic thiosemicarbazone Fe(III) complex: characterization of its antitumor activity and identification of anticancer mechanism, *Eur. J. Med. Chem.* 123 (2016) 354–364.
- [42] K.B. Huang, Z.F. Chen, Y.C. Liu, Z.Q. Li, J.H. Wei, M. Wang, X.L. Xie, H. Liang, Platinum(II) complexes containing aminophosphonate esters: synthesis, characterization, cytotoxicity and action mechanism, *Eur. J. Med. Chem.* 64 (2013) 554–561.
- [43] J. Wang, J. Yi, Cancer cell killing via ROS: to increase or decrease, that is the question, *Canc. Biol. Ther.* 7 (2008) 1875–1884.
- [44] X.C. Huang, R.Z. Huang, Z.X. Liao, Y.M. Pan, S.H. Gou, H.S. Wang, Synthesis and pharmacological evaluation of dehydroabietic acid thiourea derivatives containing bisphosphonate moiety as an inducer of apoptosis, *Eur. J. Med. Chem.* 108 (2016) 381–391.
- [45] S.H. Huang, L.W. Wu, A.C. Huang, C.C. Yu, J.C. Lien, Y.P. Huang, J.S. Yang, J.H. Yang, Y.P. Hsiao, W.G. Wood, C.S. Yu, J.G. Chung, Benzyl isothiocyanate (BITC) induces G2/M phase arrest and apoptosis in human melanoma A375.S2 cells through reactive oxygen species (ROS) and both mitochondria-dependent and death receptor-mediated multiple signaling pathways, *J. Agric. Food Chem.* 60 (2012) 665–675.
- [46] M. Kamachi, T.M. Le, S.J. Kim, M.E. Geiger, P. Anderson, P.J. Utz, Human autoimmunity sera as molecular probes for the identification of an autoantigen kinase signaling pathway, *J. Exp. Med.* 196 (2002) 1213–1225.
- [47] M.C. Wei, W.X. Zong, E.H.Y. Cheng, T. Lindsten, V. Panoutsakopoulou, A.J. Ross, K.A. Roth, G.R. MacGregor, C.B. Thompson, S.J. Korsmeyer, Proapoptotic Bax and Bak: a requisite gateway to mitochondrial dysfunction and death, *Science* 292 (2001) 727–730.
- [48] Z.M. Wang, H.Y. Yu, S.H. Gou, F.H. Chen, L. Fang, Design, synthesis, and biological features of platinum(II) complexes with rigid steric hindrance, *Inorg. Chem.* 55 (2016) 4519–4528.
- [49] J.X. Qi, Y. Gou, Y. Zhang, K. Yang, S.F. Chen, L. Liu, X.Y. Wu, T. Wang, W. Zhang, F. Yang, Developing anticancer ferric prodrugs based on the N-donor residues of human serum albumin carrier IIA subdomain, *J. Med. Chem.* 59 (2016) 7497–7511.
- [50] Y.J. Qin, Y.J. Li, A.Q. Jiang, M.R. Yang, Q.Z. Zhu, H. Dong, H.L. Zhu, Design, synthesis and biological evaluation of novel pyrazoline containing derivatives as potential tubulin assembling inhibitors, *Eur. J. Med. Chem.* 94 (2015) 447–457.
- [51] J.Y. Zhang, T. Yi, J. Liu, Z. Zhao, H.B. Chen, Quercetin induces apoptosis via the mitochondrial pathway in KB and KBv200 cells, *J. Agric. Food Chem.* 61 (2013) 2188–2195.
- [52] A.V. Schofield, C. Gamell, R. Suryadinata, B. Sarcevic, O. Bernard, Tubulin Polymerization promoting protein 1 (Tppp1) phosphorylation by rho-associated coiled-coil Kinase (Rock) and cyclin-dependent kinase 1 (Cdk1) inhibits microtubule dynamics to increase cell proliferation, *J. Biol. Chem.* 288 (2013) 7907–7917.
- [53] P.B. Schiff, J. Fant, S.B. Horwitz, Promotion of microtubule assembly *in vitro* by paclitaxel, *Nature* 227 (1979) 665–667.